iScience

CellPress
OPEN ACCESS

Article

Fluid shear stress-modulated chromatin accessibility reveals the mechano-dependency of endothelial SMAD1/5-mediated gene transcription

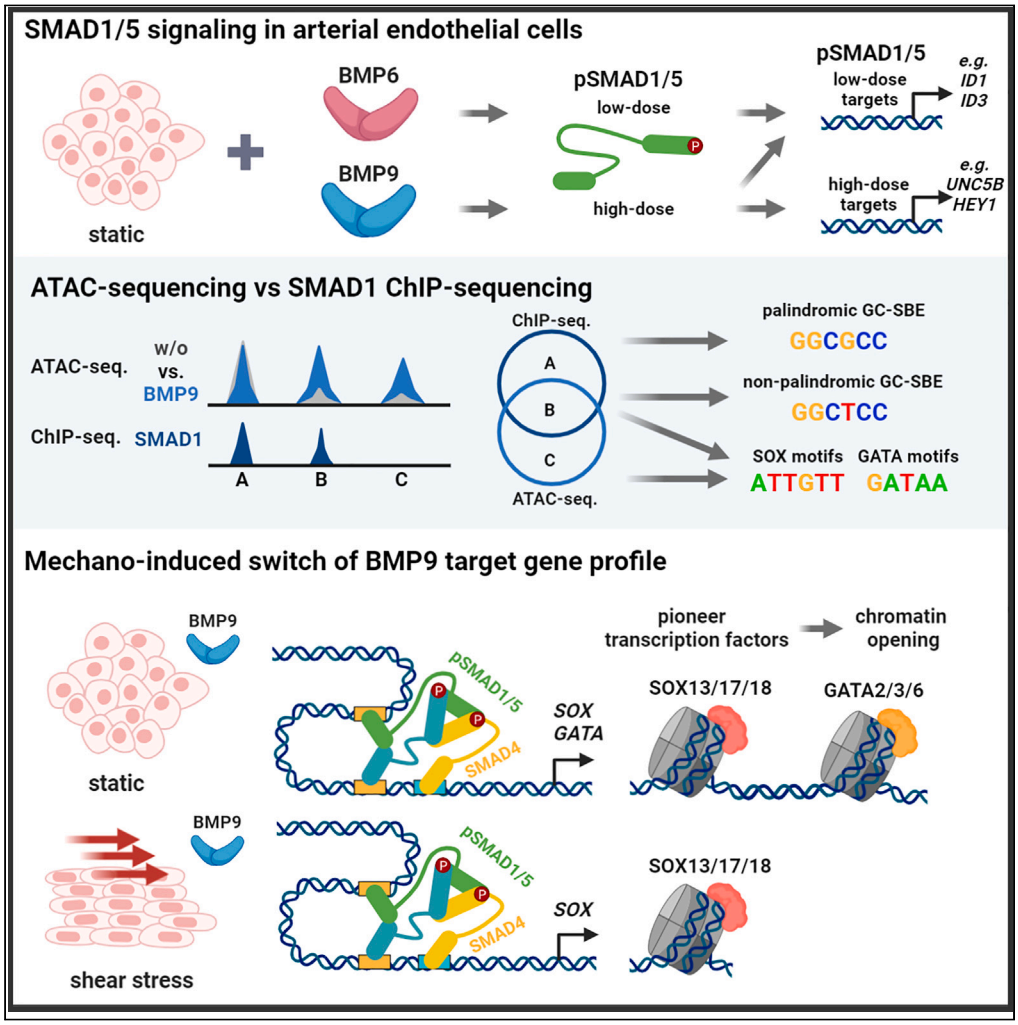

Jerome Jatzlau, Paul-Lennard Mendez, Aybuge Altay, ..., Stefan Mundlos, Martin Vingron, Petra Knaus

petra.knaus@fu-berlin.de

Highlights

High and low doses of activated SMAD1/5 differentially regulate target genes

SOX(13/18) and GATA(2/3/6) are direct SMAD1/5 targets

BMP9-sensitive chromatin regions are enriched for npGC-SBE, SOX, and GATA motifs

FSS induces a switch from SOX/GATA to SOX-only motifs in BMP9-sensitive regions

Jatzlau et al., iScience 26, 107405
September 15, 2023 © 2023
https://doi.org/10.1016/j.isci.2023.107405

iScience

CellPress
OPEN ACCESS

Article

Fluid shear stress-modulated chromatin accessibility reveals the mechano-dependency of endothelial SMAD1/5-mediated gene transcription

Jerome Jatzlau,[1,2,3] Paul-Lennard Mendez,[1,3,4,6] Aybuge Altay,[3,6] Lion Raaz,[1,3,4,5] Yufei Zhang,[3] Sophia Mähr,[1] Akin Sesver,[1] Maria Reichenbach,[1] Stefan Mundlos,[3,4,5] Martin Vingron,[3,4] and Petra Knaus[1,2,4,7,*]

SUMMARY

Bone morphogenetic protein (BMP) signaling and fluid shear stress (FSS) mediate complementary functions in vascular homeostasis and disease development. It remains to be shown whether altered chromatin accessibility downstream of BMP and FSS offers a crosstalk level to explain changes in SMAD-dependent transcription. Here, we employed ATAC-seq to analyze arterial endothelial cells stimulated with BMP9 and/or FSS. We found that BMP9-sensitive regions harbor non-palindromic GC-rich SMAD-binding elements (GGCTCC) and 69.7% of these regions become BMP-insensitive in the presence of FSS. While GATA and KLF transcription factor (TF) motifs are unique to BMP9- and FSS-sensitive regions, respectively, SOX motifs are common to both. Finally, we show that both SOX(13/18) and GATA(2/3/6) family members are directly upregulated by SMAD1/5. These findings highlight the mechano-dependency of SMAD-signaling by a sequential mechanism of first elevated pioneer TF expression, allowing subsequent chromatin opening to eventually providing accessibility to novel SMAD binding sites.

INTRODUCTION

Blood flow through the vascular network generates mechanical forces, as fluid shear stress (FSS), exerted on endothelial cells (ECs).[1] FSS has been shown to induce drastic transcriptomic and epigenetic cellular responses in ECs[2–6] and diversely integrate into cellular signaling pathways, such as the bone morphogenetic protein (BMP) and transforming growth factor β (TGFβ) pathways.[7–9]

BMPs were shown to regulate angiogenesis and vascular homeostasis. Hence, dysregulation of signaling can lead to severe vascular diseases.[10,11] Several members of the BMP ligand family are found in human plasma (BMP2, 4, 6, 7, 9, and 10) with distinct roles in regulating vascular functions, dependent on the expression of their corresponding high affinity receptors.[11–14] In ECs, BMP6 signaling leads to transcription of only a limited set of SMAD1/5 target genes (e.g., *ID1*, *ID2*, *HES1*),[15] while BMP9 signaling was reported to be more potent and induces a broad variety of additional SMAD1/5 targets (e.g., *HEY1*, *HEY2*, *JAG1*, *VEGFR1*, *GJA5*, *OCLN*).[16–19] These additional SMAD1/5 target genes are associated with endothelial quiescence[19–21] and underline that different BMPs can induce distinct biological functions in the vasculature.

SMADs have been shown to bind to distinct DNA motifs via their MH1 domain.[22] Initially, TGFβ R-SMADs 2/3 and SMAD4 were reported to bind GTCT(C/G) motifs, also called SMAD binding elements (SBEs).[23–27] More recently, all R-SMADs and SMAD4 were found to recognize 5GC motifs as well as SBE sites although R-SMADs 2/3 and SMAD4 binds as monomers whereas SMAD1/5/8 recognize these sites as dimers.[26,28] ChIP-seq experiments revealed the occurrence of two different forms of GC-SBEs: (1) a palindromic GC-SBE (pGC-SBE; GGCGCC), which was enriched in SMAD1-bound regions common to different cell types, and (2) a non-palindromic GC-SBE (npGC-SBE; GGCTCC), which was associated with cell type specific SMAD1-bound regions. Interestingly, reporter gene experiments revealed that stimulation with either BMP6 or BMP9 of reporters containing pGC-SBE-motifs lead to higher activity than those containing npGC-SBE.[16]

A special group of DNA binding factors, termed pioneer transcription factors (TFs), can bind to nucleosomal DNA and make it accessible for subsequent binding of other TFs.[29] Recently, it was shown that

[1]Institute of Chemistry and Biochemistry - Biochemistry, Freie Universität Berlin, 14195 Berlin, Germany

[2]Berlin-Brandenburg School for Regenerative Therapies (BSRT), 13353 Berlin, Germany

[3]Max Planck Institute for Molecular Genetics, 14195 Berlin, Germany

[4]International Max-Planck Research School for Biology AND Computation (IMPRS-BAC), 14195 Berlin, Germany

[5]Institute of Medical and Human Genetics, Charité Universitätsmedizin, 13353 Berlin, Germany

[6]These authors contributed equally

[7]Lead contact

*Correspondence: petra.knaus@fu-berlin.de

https://doi.org/10.1016/j.isci.2023.107405

SOX13, a member of the SOX pioneer TF family,[30] is robustly upregulated by FSS and suppresses pro-inflammatory gene expression.[31] Similarly, pioneer TF KLF4 mediates vasculo-protective gene expression in response to FSS.[32] On the other hand, GATA TFs have been shown to be upregulated by atheroprone FSS.[33] Interestingly, SMADs have been shown to cooperate with a wide set of pioneer factors, including ETS and GATA TFs.[34] However, detailed analysis of SMAD-pioneer factor DNA binding dependencies in response to BMPs and FSS are lacking.

Therefore, we applied assay for transposase accessible chromatin followed by sequencing (ATAC-seq)[35] to assess TF motif enrichment in BMP9 and FSS stimulated ECs. Regions that display enhanced accessibility upon BMP9 stimulation are enriched for non-palindromic GC-SBE motif GGCTCC. Further, we observed an FSS dependent switch from SOX and GATA to SOX-only motif enrichment in BMP9-sensitive regions, demonstrating context dependent regulation of BMP9-sensitive regions.

RESULTS

BMP9 but not BMP6 selectively enhances expression of pSMAD1/5 high-dose target genes in arterial ECs

Both BMP9 and BMP6 are systemic BMPs with distinct functions on ECs,[15,36–38] however BMP9 is biologically active by inducing C-terminal phosphorylation of SMAD1/5 at pM concentrations while BMP6 is active in the nanomolar range.[15,16,39–41] We therefore performed a comparative study for both ligands in human umbilical arterial endothelial cells (HUAECs) in their respective activity range, i.e., 5nM for BMP6 and 0.3 nM for BMP9 (Figure 1A) and investigated the phosphorylation of SMAD1/5 (pSMAD1/5). Over a time-course of 2 h, BMP9 strongly increased pSMAD1/5 while BMP6 showed only a mild induction (Figure 1B). This is in line with higher expression of BMP9-high affinity receptor ALK1 compared to BMP6-high affinity receptor ALK2 (S1A-B).[41,42] We next investigated the transcriptional regulation of known BMP-SMAD1/5 target genes after 2 h ligand stimulation. While both ligands led to a similar induction of some target genes, i.e., *ID1* and *ID3* (Figures 1C and S1C), BMP9 stimulation led to a more prominent upregulation of other target genes when compared to BMP6, i.e., *UNC5B, ID2, HEY1,* and *SNAI1* (Figures 1D and S1D). Differential target gene regulation was confirmed in human aortic ECs (Figure S2A). Consequently, SMAD targets were grouped into pSMAD1/5 low-dose and high-dose target genes, which are responsive to low or high levels of phosphorylated SMADs as elicited by BMP6 or BMP9. SMAD1/5 dependency could be confirmed by siRNA depletion for members of both low- and high-dose targets, i.e., *ID1* and *UNC5B* (Figures 1D and S1E). Finally, we tested if these effects are also seen on protein level. In line with the transcriptional effects, ID1 protein levels were similarly regulated by BMP9 or BMP6 (Figures 1E, 1F, and S1F). In contrast, UNC5B protein sequentially followed strong SMAD1/5 phosphorylation induced by BMP9 only (Figures 1E, 1F, S1F, and S1G). In summary, in HUAECs BMP6 and BMP9 can elicit distinct transcriptional responses dependent on the levels of SMAD1/5 phosphorylation. Accordingly, pSMAD1/5 high-dose target genes such as *UNC5B* respond to strong SMAD1/5 phosphorylation as induced by BMP9 but not BMP6, while pSMAD1/5 low-dose target genes like *ID1* are equally induced by either of both BMP ligands.

pSMAD1/5 high-dose target regions require chromatin opening

BMP9-dependent regulation of target genes plays a crucial role in the physiological homeostasis of vascular ECs but is equally associated with patho-physiological processes.[19,20,43] To get deeper insights in BMP9 regulation of target genes we used ATAC-seq and identified genomic chromatin accessibility depicting active (open) chromatin regions upon BMP9 stimulation of HUAECs. We found that BMP9 stimulation leads to a prominent increase in accessibility compared to control (n = 15087 for opening versus n = 8180 for closing regions) (Figure 2A). Interestingly, increased chromatin accessibility was prominent in pSMAD1/5 high-dose target *UNC5B* in a SMAD1/5 bound region (Regulatory region 22, Rr 22) while other SMAD1/5 bound regions in the gene locus showed no differential accessibility (Figure 2B, upper panel). Intriguingly, when we cloned the respective SMAD1/5 bound regions into luciferase-based reporter gene constructs, only Rr 22 led to a significant increase in luciferase activity in HEK293T cells stimulated with BMP6, which is more potent than BMP9 in inducing SMAD1/5 dependent BRE_2-reporter activity in these cells (Figures S3A and S3B). In contrast to *UNC5B*, we didn't observe any significant changes in chromatin accessibility in the locus of pSMAD1/5 low-dose target *ID1* (Figure 2B, lower panel). We next defined BMP-sensitive regions (BSRs) as the regions that show increased accessibility upon BMP treatment and compared the overlap of BSRs with published SMAD1-bound regions (SBRs) as identified by SMAD1 ChIP-seq.[16,44] Out of 23,627 BSRs, 596 overlapped with BMP9-induced SBRs in HUVECs and 1719 SBRs in BMP9 stimulated HPAECs (Figure 2C). Subsequently, we applied enrichment analysis to attribute

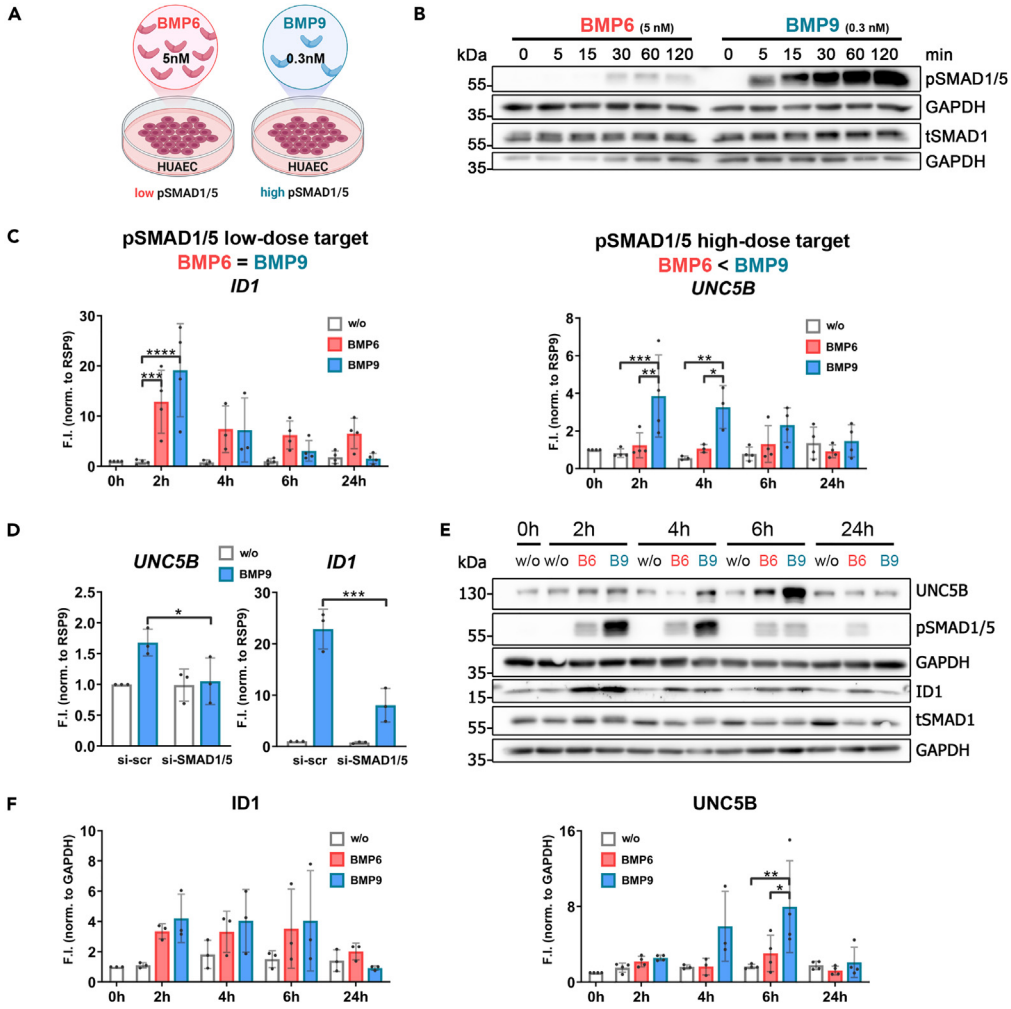

Figure 1. BMP6 and BMP9 differentially regulate pSMAD1/5 low- and high-dose target genes

(A) In all panels, HUAECs were stimulated for the indicated time points with either BMP6 (5 nM) or BMP9 (0.3 nM) after 3 h of starvation. Low (BMP6) or high (BMP9) SMAD1/5 phosphorylation was detected by immunoblot using respective antibodies.

(B) Immunoblot showing short-term (up to 2 h) BMP6 or BMP9 responses on HUAECs using antibodies against phospho (p)SMAD1/5, total (t)SMAD1 and GAPDH (representative blot, n = 3 independent experiments).

(C) qRT-PCR showing expression of pSMAD1/5 low-dose target gene *ID1*, characterized by equal induction downstream of BMP6 and BMP9, and pSMAD1/5 high-dose target gene *UNC5B* characterized by higher BMP9 induction. Values are expressed as mean fold induction (F.I.) ±SD (n = 3–4 independent experiments).

(D) After 2 days of siRNA treatment (scrambled control, siSMAD1 or siSMAD5), HUAECs were stimulated with BMP9 for 2 h. qRT-PCR shows decreased *UNC5B* and *ID1* induction in the absence of SMAD1/5. Values are expressed as mean fold induction (F.I.) ±SD (n = 3 independent experiments).

(E) Immunoblot showing long-term (up to 24 h) BMP6 and BMP9 response on HUAECs using antibodies against UNC5B, pSMAD1/5, ID1, tSMAD1 and GAPDH (representative blot of n = 3).

(F) Densitometric quantification of UNC5B and ID1 relative to GAPDH levels expressed as mean fold induction (F.I.) ±SD in arbitrary units (AU) (n = 3–4). Statistical significance within groups (C,F) or relative to si-scr (D) was calculated using two-way ANOVA and Tukey's post-hoc test.; *p < 0.05, **p < 0.01, ***p < 0.001, ****p < 0.0001. See also Figure S1 and S2.

functional significance to the regions gaining and losing activities upon BMP9 stimulation using GREAT.[45] Interestingly, regions activated by BMP9 stimulation were, *inter alia*, associated with the GO term *pathway-restricted SMAD phosphorylation* (Figure 2D), supporting the suitability of our approach. We next asked which TFs might drive the genomic changes upon BMP9 treatment and performed motif enrichment analysis using HOMER.[46] We found that BMP9-sensitive, active regions were mostly enriched for GATA and SOX pioneer TF motifs (Figure 2E). Furthermore, using *de novo* motif analysis, we detected two motifs

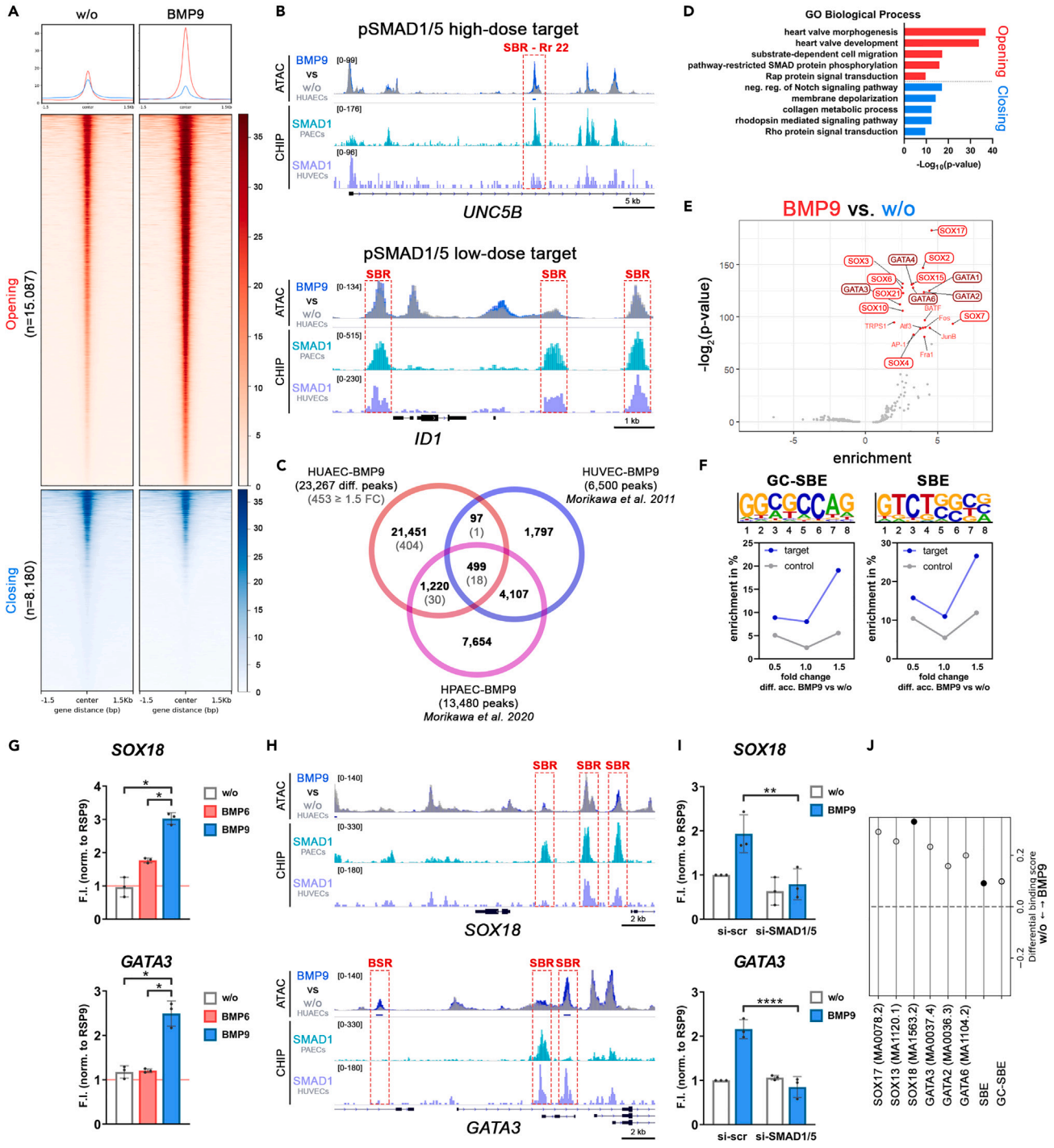

Figure 2. ATAC-Seq identifies pSMAD1/5 high-dose targets

(A) Heatmap and intensity profile depicting ATAC-seq coverage of BMP9-induced opening and closing regions in HUAECs 2 h after BMP9 stimulation.

(B and H) Genome browser view of ATAC-seq and two publicly available BMP9-stimulated vascular SMAD1 ChIP-seq datasets (GSM2805410/1, GSM684747) on (B) *UNC5B* and *ID1* locus and (H) *SOX18* and *GATA3* locus. SBR – SMAD1 bound region, identified by overlapping ChIP-seq signals. BSR – BMP9-sensitive region, identified by increased ATAC-seq signal in BMP9 vs. unstimulated (w/o) HUAEC.

(C) Venn diagram depicting overlaps in BMP9-sensitive regions (BSRs) from ATAC-seq and SBRs identified by ChIP-seq.

(D) Gene Ontology enrichment analysis of opening and closing BSRs. Data was produced using GREAT tool.

(E) Volcano plot, highlighting significantly enriched motifs in ATAC-seq opening versus closing regions (FC ≥ 1.5) found by HOMER tool. Pioneer transcription factor SOX and GATA families are significantly enriched (highlighted in bold).

Figure 2. *Continued*

(F) Enrichment of *de-novo* predicted GC-SBE- and SBE-like motifs in peaks with different fold changes between BMP9 and unstimulated ATAC-seq peaks.
(G) qRT-PCR showing expression of pSMAD1/5 high-dose target genes *SOX18* and *GATA3* characterized by higher BMP9 vs. BMP6 induction. Values are expressed as mean fold induction (F.I.) ±SD (n = 3 independent experiments).
(I) After 2 days of siRNA treatment (scrambled control, siSMAD1 or siSMAD5) HUAECs were stimulated with BMP9 for 2 h. qRT-PCR shows no *SOX18* and *GATA3* induction in the absence of SMAD1/5. Values are expressed as mean fold induction (F.I.) ±SD (n = 3 independent experiments).
(J) Scatterplot of footprint scores for SOX13/17/18, GATA2/3/6, GC-SBE & SBE motifs shows elevated differential binding score in BMP9 vs. w/o. Filled dot indicates top 5 ranking TFs. Statistical significance within groups (G) or relative to si-scr (I) was calculated using two-way ANOVA and Tukey's post-hoc test.; *p < 0.05, **p < 0.01, ***p < 0.001. See also Figures S2, S3, S4 and S5.

which harbor the previously reported GC-rich SMAD binding element (GC-SBE)[16] or the SBE motif (GTCTG/CAGAC).[47] Both the GC-SBE-like motif as well as the SBE-like motif were enriched (19.1% versus 5.59% baseline, 26.65% versus 11.97% baseline) in BMP9-sensitive active regions compared to controls (fold change >1.5) (Figure 2F). A recent study highlighted that short variations of the GC-SBE (5bp GC-SBEs) are clustered in SMAD1 ChIP-seq peaks,[22] thereby likely allowing sufficient binding of trimeric SMAD complexes. We investigated occurrence and clustering of GC-SBEs, 5bp GC-SBEs and SBEs in BMP9-induced active regions in a similar manner. However, less than 10% of differential ATAC-seq peaks contained GC-SBEs or 5 bp GC-SBEs, and less than 20% harbored SBE motifs, while neither of them was prominently clustered (Figure S3C). Interestingly, the relative occurrence of pGC-SBE to npGC-SBE was prominently lower in ATAC-seq (1:8.4; 0.7%/5.89%) compared to ChIP-seq (3.2:1; 99.75%/30.82%) peaks. (Figure S3C).

Next, we validated which GATA and SOX family members could account for increased SOX/GATA binding in BMP9-sensitive regions. Collectively, *GATA2/3/6* as well as *SOX13/17/18* were differentially regulated on a transcript level 2 h after BMP9 stimulation (Figures 2G and S4A). This is in line with SMAD1-binding in proximity or within the *GATA2/3* and *SOX13/18* loci (Figures 2H and S4B). Furthermore, we observed a loss (*GATA3* and *SOX18)* or reduction *(GATA2,6* and *SOX13)* of BMP9-responsiveness upon siRNA mediated depletion of SMAD1/5. (Figures 2I and S4C). Finally, we complemented our motif enrichment analysis with TF footprinting analysis, both for BMP9 induced and control samples using TOBIAS.[48] We observed footprints of SOX and GATA binding sites as well as GC-SBE and SBE motifs in BMP9-induced ATAC peaks, indicating SMAD, SOX and GATA occupancy within BSRs (Figures 2J and S4D–S4F).

We further investigated the BSR regions containing GC-SBE footprints (GC-SBE$^+$) and found that half of them harbored npGC-SBEs in proximity to SBEs (npGC-SBE$^+$, 51,9%) (Figure S5A). In contrast to pSMAD1/5 low-dose target genes *ID1/2/3* which harbor composite motifs of a palindromic GC-SBE and SBE with a motif spacer of 5 bp,[16] potential npGC-SBE composite motifs were characterized by varying spacer lengths from 3 to 17bp (Figure S5A). Interestingly, 60.7% of npGC-SBE$^+$ peaks contained also at least one SOX motif (SOX-motif$^+$), while 34,3% carried a GATA motif (GATA-motif$^+$) and collectively 75,5% harbored either an SOX or a GATA motif. For example, BSRs carrying npGC-SBE footprints together with SOX or GATA footprints were found in proximity of the *MAL2*, *PRICKLE2* and *SGK1* loci, which all showed stronger upregulation by BMP9 compared to BMP6 on transcript level, characteristic of known pSMAD1/5 high-dose target genes (*HEY1*, *UNC5B* and *SNAI1)* (Figures 1C and S5B). Finally, we validated that BMP9-dependent upregulation of *GATA2/3/6* and *SOX13/17/18* is also seen in human aortic ECs, suggesting a common endothelial BMP9 responsiveness of these TFs (Figure S2B).

Taken together, BMP9 induces SOX13/18 and GATA2/3/6 in a SMAD1/5-dependent manner and BMP9-sensitive active regions mostly harbor SOX and GATA motifs together with SMAD binding sites. These GC-SBE$^+$ BSRs (1) carry mostly npGC-SBE (GGCTCC) motifs, (2) lack SBE clustering and (3) contain composite motifs with a variable spacer distance.

FSS as modulator of BMP9-target gene regulation

FSS fine-tunes vascular BMP signaling with studies showing that it potentiates BMP9 responses in ECs.[9,49,50] We were therefore interested if FSS and BMP9 co-regulate expression of pSMAD1/5 high-dose target genes. We exposed HUAECs to FSS of 30 dyn/cm^2 for 2 or 6 h (RNA & ATAC-seq samples 2 h; protein samples 2 & 6 h) using a pneumatic pump system (Figure 3A). We observed alignment of HUAECs along the direction of flow for both time-points (Figure S6A) and the induction of flow-responsive pioneer TF *KLF2* (Figure 3B),[51] validating our flow set-up. We next performed ATAC-seq of FSS exposed HUAECs and could similarly observe a strong increase in accessibility downstream of the *KLF2* locus

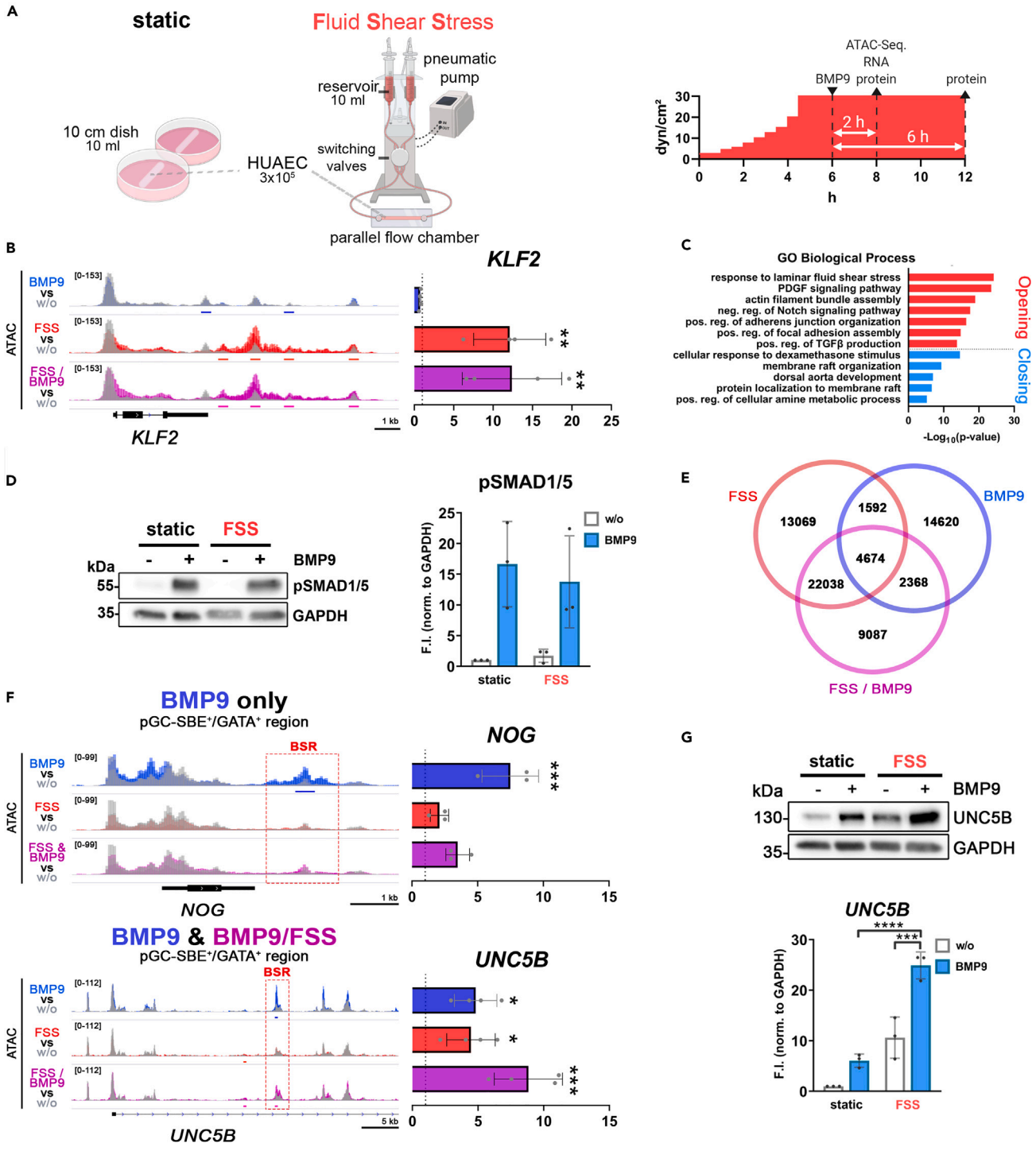

Figure 3. Fluid Shear Stress modulates BMP9-dependent regulation of chromatin accessibility

(A) Scheme depicting Fluid Shear Stress (FSS) set-up (left) and the applied shear regime (right).

(B–G) HUAECs were allowed to adapt for 6 h to 30 dyn/cm^2 in EBM2 with 1% FCS and stimulated with or without BMP9 (0.3 nM) for 2 h for ATAC-seq. and RNA analysis, or 6 h for protein analysis with and without FSS. (B) Genome browser view of BMP9, FSS and BMP9/FSS ATAC-seq data on *KLF2* locus and qRT-PCR showing *KLF2* expression after 2 h of the respective stimulation. Values are expressed as fold induction (F.I.) ±SD relative to static w/o BMP9 (n = 4 independent experiments). (C) Gene Ontology enrichment analysis of FSS ATAC-seq data for opening and closing regions. Data was produced using GREAT tool. (D) Immunoblot of phosphorylated SMAD1/5 after 2 h of BMP9 stimulation with and without FSS with the respective densitometric quantification expressed as mean fold induction (F.I.) ±SD in arbitrary units (AU) (n = 3 independent experiments). (E) Venn diagram showing overlap of

Figure 3. *Continued*
differentially accessible regions of BMP9, FSS and BMP9/FSS ATAC-seq compared to untreated cells. (F) Genome browser view of BMP9, FSS and BMP9/FSS ATAC-seq data on *NOG* and *UNC5B* locus and qRT-PCR showing gene expression after 2 h of the respective stimulation. Values are expressed as fold induction (F.I.) ±SD relative to static w/o BMP9 (n = 3 *NOG*, n = 4 *UNC5B*; independent experiments). (G) Immunoblot showing UNC5B levels after 6 h of FSS stimulation with or without BMP9 stimulation (representative blot, n = 3) and (lower) densitometric quantification of UNC5B relative to GAPDH levels expressed as mean fold induction (F.I.) ±SD in arbitrary units (AU) (n = 3). Statistical significance compared to static w/o BMP9 was calculated using one-way ANOVA and Dunnett's post-hoc test (B, F) or two-way ANOVA and Šídák's post-hoc test (G).; *p < 0.05, **p < 0.01, ***p < 0.001, ****p < 0.0001. See also Figures S6 and S7.

(Figure 3B). Overall, FSS led to both activation and inactivation of chromatin regions (n = 21,857 for opening, n = 19,546 for closing regions) (Figure S6B). Subjecting differentially accessible regions to GREAT for functional annotation,[45] we found that FSS-sensitive active regions were associated with the term *response to fluid shear stress*, highlighting the suitability of ATAC-seq data to analyze cellular responses to FSS (Figure 3C). Using HOMER motif enrichment analysis, we found that FSS-sensitive active regions were mostly enriched for KLF and SOX TF family motifs, whereas the regions losing their activity carry ETV/ETS and TEAD family motifs (Figure S6C).

Next, we evaluated whether FSS alters BMP9 induced SMAD1/5 phosphorylation, but we observed no significant differences between these conditions (Figure 3D). Subsequently, we compared accessibility profiles of the cells stimulated with only BMP9, only FSS, or a combination of both (BMP9/FSS). Strikingly, we observed that out of 23,254 regions differentially regulated upon BMP9 stimulation under static conditions, only 7,042 (30.28%) regions were shared upon simultaneous BMP9 and FSS stimulation, while more than 9,000 regions were unique to the BMP9/FSS condition (Figure 3E). This is in line with GC-SBE and SBE footprints being enriched in FSS-induced closing regions, suggesting an inhibitory effect of FSS on BMP9-induced SMAD1/5 target gene regulation (Figure S6D).

Exemplarily, a pGC-SBE$^+$ & GATA-motif$^+$ BSR downstream of the *NOG locus* showed a strong increase in accessibility upon BMP9 stimulation under static conditions, which was lost if exposed to BMP9/FSS, as also validated by *NOG* mRNA levels (Figures 3F and S7A). In contrast, *UNC5B* locus harbors a pGC-SBE$^+$ & GATA-motif$^+$ region (Rr 22) that was inducible by both BMP9 and BMP9/FSS. Accordingly, expression levels of *UNC5B* were significantly elevated upon stimulation with BMP9, FSS and BMP9/FSS stimulation (Figures 3F and S7A). Similarly, protein levels of UNC5B were significantly higher after BMP9/FSS stimulation compared to BMP9 or FSS only stimulations (Figure 3G). Taken together, we show that FSS drastically alters BMP9 induced chromatin changes and that FSS can act either synergistically or antagonistically on BMP9-SMAD1/5 signaling.

BMP9 and FSS collectively regulate chromatin accessibility

In order to get deeper insights into co-regulation of target genes in BMP9/FSS, we analyzed regions that were closing (n = 903, Cat a) or opening (n = 3158, Cat d) upon both BMP9 and FSS, closing upon BMP9 and opening upon FSS (n = 950, Cat b) or opening after BMP9 stimulation but closing after FSS stimulation (n = 1270 Cat c) (Figure 4A). We next annotated biological functions of genomic regions in Cat a and d using GREAT. In Cat a, regions were associated with terms *regulation of actin cytoskeleton organization*, *angiogenesis* or *negative regulation of notch signaling* (Figure 4B). More interestingly, regions in Cat d were associated with terms *pathway-restricted SMAD phosphorylation* and *positive regulation of TGFβ receptor signaling pathway* (Figure 4B) reflecting on the complex co-regulation of BMP9 and FSS on pSMAD1/5 high- and low-dose target genes. Next, we performed TF motif enrichment analysis in regions differentially accessible in BMP9/FSS against unstimulated control using HOMER. We found SOX, BACH, and FOS/JUN TF motifs to be enriched in activated regions while ETS/ETV, EWS, and TEAD TF family were enriched in inactivated regions (Figure 4C). Accordingly, we observed that BMP9, FSS or BMP9/FSS stimulation led to enhanced accessibility of a npGC-SBE$^+$/SOX-motif$^+$ BSR upstream of *SPSB1*, accompanied by elevated expression of *SPSB1* (Figures 4D and S7B). In contrast a npGC-SBE$^+$/ETS-motif$^+$ BSR upstream of *BCAR1* showed reduced accessibility in line with decreased expression of *BCAR1* in all three conditions (Figures 4D and S7B). Finally, we investigated the expression of SOX and GATA TFs in the presence and absence of FSS. We found that FSS inhibited BMP9-induced expression of *GATA2/3/6* while BMP9 induced expression of *SOX13/17/18* was either similarly strong (*SOX13/18*) or elevated (*SOX17*) by additional FSS stimulation (Figures 4E and S8). Collectively, this suggests a BMP9-dependent mechano-sensitive chromatin opening. Collectively, this suggests a BMP9-dependent mechano-sensitive chromatin opening, including

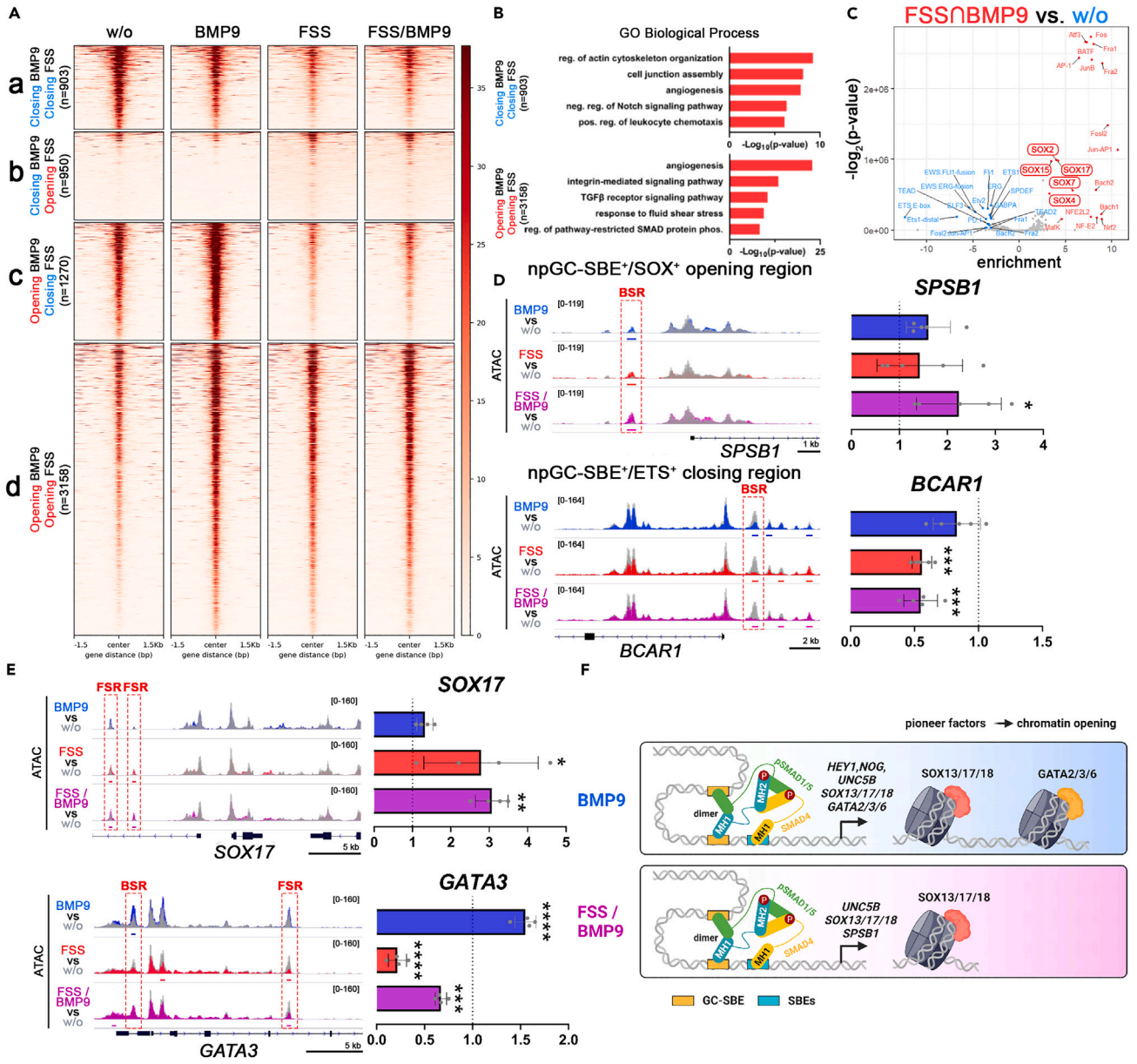

Figure 4. Fluid Shear Stress and BMP9 co-regulate chromatin accessibility

(A) Heatmaps depicting ATAC-seq coverage in regions opening and closing in the same or opposite way in BMP9, FSS and BMP9/FSS ATAC-seq regions.

(B) Gene Ontology enrichment analysis of ATAC-seq data for regions opening or closing in both, BMP9 and FSS samples. Data was produced using GREAT tool.

(C) Motif enrichment analysis of genomic regions sensitive to both, BMP9 and FSS individually using HOMER tool. Pioneer transcription factor SOX family is significantly enriched (highlighted in bold).

(D and E) Genome browser view of BMP9, FSS and BMP9/FSS ATAC-seq data on (D) *SPSB1* and *BCAR1* loci (E) *SOX17* and *GATA3* loci and qRT-PCR showing gene expression after 2 h of the respective stimulation. Values are expressed as fold induction (F.I.) ±SD relative to static w/o BMP9 (n = 4–5 independent experiments). BSR – BMP9 sensitive region, FSR – Fluid Shear Stress sensitive region. Statistical significance compared to static w/o BMP9 was calculated using one-way ANOVA and Dunnett's post-hoc test.; *p < 0.05, **p < 0.01, ***p < 0.001, ****p < 0.0001.

(F) BMP9-induced pSMAD1/5 regulates expression of SMAD target genes including pioneer transcription factors GATA2/3/6 and SOX13/17/18, which consequently promote chromatin opening. Under Fluid Shear Stress (FSS) application, many target genes including the GATA2/3/6 family become inaccessible for SMADs, whereas SOX TFs remain BMP9-sensitive. See also Figures S7 and S8.

transcriptional regulation by SOX (FSS) or SOX and GATA (FSS and BMP9) pioneer TFs. Whether this transcriptional regulation depends on their pioneering function remains to be determined (Figure 4F).

Taken together, we present here the first comprehensive analysis of motifs enriched in genomic regions regulated by BMP9/FSS and thoroughly analyzed SMAD TF binding in BMP9-sensitive regions. We could show that ATAC-seq is a powerful and versatile technique suitable to deepen our understanding of BMP-induced gene regulation mediated by SMAD and non-SMAD TFs. Further, combination of BMP-stimulation with physiological relevant mechano-regimes such as FSS highlights the context dependent regulation of SMAD signaling by mechano-sensitive pathways.

DISCUSSION

The BMP family of growth factors is comprised of a plethora of members which, upon binding to specific receptors, induce downstream phosphorylation, i.e., activation, of SMAD1/5 TFs[52,53] Still, different BMP ligands induce distinct sets of target genes, raising the question how this differential transcriptional regulation arises from activation of the same TFs. It has been suggested that these transcriptional outcomes can be fine-tuned by different affinities of SMAD TFs to target regions[16] in addition to induction of non-SMAD signaling and regulation via co-regulators.[53] The MH1 domain of SMADs possess a weak DNA binding affinity[23] and previous comparative studies showed that these are in a similar nanomolar range for different SMAD motifs.[22] Further it was discussed that a heterotrimeric SMAD complex would gain affinity through binding to two or three SBEs simultaneously, as suggested for the goosecoid promoter.[16,22,54] Analysis of SMAD1 binding sites via ChIP-seq revealed palindromic GC-SBE motifs in regions that are commonly bound by SMAD1 in different cell types (e.g., *ID1/2/3* loci), and non-palindromic GC-SBE motifs in cell type specific SMAD1-bound regions.[16] We add to these observations that npGC-SBE motifs are particularly associated with BMP9-sensitive active chromatin regions which carry additional pioneer co-TF binding sites as identified by ATAC-seq. Genes in vicinity to those npGC-SBE$^+$ BSRs were only regulated in the presence of saturating pSMAD1/5 levels (high-dose), highlighting a mechanism which governs a pSMAD1/5-dose-dependent target gene regulation. Based on our observations, we envisage a mechanism in which low levels of pSMAD1/5 are capable of binding to pGC-SBE composite motifs in open chromatin regions. However, regulating target genes in npGC-SBE$^+$ genomic regions requires the cooperation of SMAD1/5 and pioneering TF activity, which facilitate the opening of chromatin. Similarly, SMAD2/3-dependent regulation of mesoderm differentiation genes was associated with SMAD2/3 binding to pioneer TF FoxH1.[34,55]

In this study, we further showed that in arterial ECs pioneer TFs GATA2/3 and SOX13/18 are directly regulated by SMAD1/5 on transcript level. This suggests that SMAD1/5 target regulation might occur in two phases: (1) an immediate response where pSMAD1/5 bind to open chromatin regions with palindromic GC-SBE composite motifs, including pioneer TFs SOX and GATA and (2) SOX and GATA bind and open closed chromatin regions and regulate secondary target gene transcription independently or together with pSMAD1/5 (e.g., *UNC5B, SGK1, PRICKLE2*).

Analyzing BMP9-induced chromatin accessibility under different physiological or pathological conditions such as the presence or absence of FSS allows to further identify context dependent co-TFs, which modulate BMP-SMAD signaling. ECs are constantly exposed to mechanical forces, including FSS.[56] Moreover, interplay of BMP/TGFβ signaling with various mechano-sensitive pathways and direct regulation by mechanical forces have been shown.[7,57] We therefore analyzed how BMP9 and FSS co-regulate SMAD target gene regulation on chromatin level. Interestingly, the majority of BMP9-sensitive regions found under static conditions was lost in the presence of FSS (e.g., *NOG locus*), whereas other regions remained sensitive toward BMP9 in the presence of FSS (e.g., *UNC5B intron*). As FSS reduces *GATA2/3* expression, the change in BSRs from GATA-motif$^+$/SOX-motif$^+$ in static ECs to SOX-motif$^+$ BSRs in FSS-exposed ECs likely coincides with changes in pioneer TF expression. This is in line with shared regulation of SOX13/17/18 by BMP9 and FSS. Both GATA and SOX TFs play crucial roles in EC differentiation from embryonic stem cells and maintenance of EC specific gene expression, preventing *trans*-differentiation.[58,59] While SOX TFs have been described to act during differentiation as well as to act vasoprotective in the mature endothelium, GATA TFs were shown to be upregulated by atheroprone FSS. For instance, Sox18 has been shown to regulate EC barrier integrity upon application of FSS in pulmonary arterial ECs,[60] FSS-dependent upregulation of *SOX13* was connected to suppression of pro-inflammatory gene expression[31] and *SOX17* acts as a critical regulator of vascular homoeostasis, commonly mutated in pulmonary arterial hypertension patients.[61]

In contrast, elevated levels of *GATA3* were connected to endothelial-mesenchymal transition-mediated pulmonary arterial hypertension (PAH),[62] GATA2 was shown to directly repress atheroprotective TF KLF2,[63] and *GATA1/4* expression was elevated by pulsatile oscillatory atheroprone shear stress in HUVECs.[33] In our study, static cultivated ECs resemble more an atheroprone phenotype, highlighting that previously published static BMP-stimulation EC experiments should be carefully revised when drawing conclusions about the healthy endothelium. Since SMADs have been shown to interact and be directed to target sites by SOX and GATA TFs,[64,65] in future studies, it will be of interest to focus on how vasoprotective and atheroprone fluid shear regimes could influence SMAD co-TF association and thereby target gene regulation.

Besides the differential regulation of SOX and GATA TFs, we observed a shift from ETV/ETS to KLF TFs in FSS stimulated ECs that was very recently reported to be crucial for FSS driven transcriptomic changes in human umbilical vein ECs.[2] Moreover, we identified a loss of TEAD motif enrichment upon FSS stimulation. TEAD TFs are binding partners of Yes-associated Protein (YAP) and its paralog, the transcriptional co-activator with PDZ-binding motif (TAZ).[66] YAP/TAZ are well-known for their mechano-responsiveness,[67] have been shown to integrate into BMP/TGFβ signaling,[7,68,69] and critically regulate angiogenesis and progression of vascular diseases like pulmonary hypertension or atherosclerosis.[70]

One limitation in the analysis of SMAD composite motifs is the prediction of which SMAD binding motifs might contribute to binding of an SMAD trimer. While earlier studies suggest that an SMAD trimer could efficiently bind to a hetero-composite motif (GC-SBE and SBE) with a 5 bp spacer,[16,71] a recent structural analysis of the BMP R-SMADs highlighted dimerization of SMAD1/5/8 via their MH1 domains, which renders them incapable of binding the same SBE or in proximity to each other.[28] In consequence, two MH1 domains of a SMAD1/5/8-SMAD4 hetero-trimer can occupy a hetero composite motif, whereas the contribution of a third SMAD binding motif to SMAD binding remains to be shown by future studies. Equally, (1) the limitations of SMAD complex binding toward composite motifs containing different types of GC-SBEs, and (2) the contribution of co-transcription factors or pioneer TFs in facilitating binding to favorable or less favorable SMAD1/5 target sites is still unknown.

In conclusion, we provided major insights to the understanding of BMP9-sensitive target region regulation on chromatin level. In summary, this mechanism involves different requirements for regulating gene expression in open versus closed chromatin regions carrying distinct GC-SBE motifs. We suggest that BMP9 induces chromatin opening mediated by GATA and SOX TFs downstream of SMADs. Moreover, we provided insights in FSS and BMP9 co-regulation of target gene accessibility which may serve as a substantial base for further studies on angiogenesis or vascular disease.

Limitations of the study

Future studies should place a greater emphasis on different aspects of mechano-sensitive BMP-target gene regulation. In this study we limited our analysis to human umbilical arterial ECs. Different vascular beds, such as venous, arterial, microvascular, and macrovascular ECs, may exhibit distinct responses to BMP signaling due to their specific physiological and functional characteristics. Therefore, future investigations should consider these differences and compare vascular bed-specific BMP-dependent chromatin accessibility modulation. Furthermore, there is a need for comprehensive exploration of various BMP ligands and their effects on chromatin accessibility and gene transcription. To measure direct effects, we analyzed BMP9-dependent chromatin accessibility changes after 2 h of ligand stimulation. Time-resolved studies could uncover underlying chromatin remodeling events of differentiation or *trans*-differentiation processes downstream of BMP. Along that line, it would be of great benefit to integrate chromatin accessibility data with RNA expression data to decipher the order of events and correlate chromatin accessibility changes with changes in gene expression. Finally, the role of SOX and GATA TFs as potential pioneering factors downstream of BMP9 needs to be studied in more detail.

STAR★METHODS

Detailed methods are provided in the online version of this paper and include the following:

- KEY RESOURCES TABLE
- RESOURCE AVAILABILITY
  - Lead contact

- Materials availability
- Data and code availability
- EXPERIMENTAL MODEL AND SUBJECT DETAILS
  - Cell culture
- METHOD DETAILS
  - Transient transfection with expression plasmids and siRNA
  - Cell stimulation with growth factors and SMI treatment
  - SDS-PAGE & Western-blotting
  - Quantitative real-time PCR
  - Cloning of luciferase reporter constructs
  - Dual luciferase Reportergene assay
  - Application of fluid shear stress
  - ATAC-seq
  - ATAC-seq library preparation
  - ATAC-seq data preprocessing
  - Differential accessibility analysis
  - Transcription factor motif analysis
  - Transcription factor footprinting analysis
  - Figures
- QUANTIFICATION AND STATISTICAL ANALYSIS

SUPPLEMENTAL INFORMATION

Supplemental information can be found online at https://doi.org/10.1016/j.isci.2023.107405.

ACKNOWLEDGMENTS

We thank S. Hartmann for technical support, S. Vukicevic for reagents. J.J. was supported by Einstein Center for Regenerative Therapies (ECRT). P.K. acknowledges the support from ECRT, DFG (SFB1444), and Morbus Osler Society. P.-L. Mendez and L. Raaz were supported by IMPRS-BAC. A.A. and Y.Z. are supported by DFG-funded international training group IRTG2403.

AUTHOR CONTRIBUTIONS

J.J. performed all signaling experiments, calculated the statistics and drafted the manuscript and figures.

P.M. performed shear stress experiments, performed functional annotation and visualization of the ATAC-seq data (coverage heatmaps, volcano plots), drafted the manuscript.

A.A. performed preprocessing of ATAC-seq data, applied differential accessibility, TF motif enrichment and motif occurrence analysis, commented, and contributed to the manuscript.

L.R. performed ATAC-seq experiments, commented, and contributed to the manuscript.

Y.Z. performed TF footprinting analysis.

S.Mä. supported q-PCR experiments.

A.S. supported signaling experiments.

M.R. established flow stimulation set-up and performed flow experiments.

S.Mu. advised on the experimental design and commented on the manuscript.

M.V. advised on experimental design and on bioinformatics analyses.

J.J. and P.K. designed the experiments, discussed all data, and wrote the manuscript.

DECLARATION OF INTERESTS

The authors declare no competing interest.

INCLUSION AND DIVERSITY

We support inclusive, diverse, and equitable conduct of research.

Received: November 16, 2022
Revised: April 20, 2023
Accepted: July 12, 2023
Published: July 17, 2023

REFERENCES

1. Topper, J.N., and Gimbrone, M.A., Jr. (1999). Blood flow and vascular gene expression: fluid shear stress as a modulator of endothelial phenotype. Mol. Med. Today *5*, 40–46. https://doi.org/10.1016/s1357-4310(98)01372-0.

2. Tsaryk, R., Yucel, N., Leonard, E.V., Diaz, N., Bondareva, O., Odenthal-Schnittler, M., Arany, Z., Vaquerizas, J.M., Schnittler, H., and Siekmann, A.F. (2022). Shear stress switches the association of endothelial enhancers from ETV/ETS to KLF transcription factor binding sites. Sci. Rep. *12*, 4795. https://doi.org/10.1038/s41598-022-08645-8.

3. Bondareva, O., Tsaryk, R., Bojovic, V., Odenthal-Schnittler, M., Siekmann, A.F., and Schnittler, H.J. (2019). Identification of atheroprone shear stress responsive regulatory elements in endothelial cells. Cardiovasc. Res. *115*, 1487–1499. https://doi.org/10.1093/cvr/cvz027.

4. Ajami, N.E., Gupta, S., Maurya, M.R., Nguyen, P., Li, J.Y.S., Shyy, J.Y.J., Chen, Z., Chien, S., and Subramaniam, S. (2017). Systems biology analysis of longitudinal functional response of endothelial cells to shear stress. Proc. Natl. Acad. Sci. USA *114*, 10990–10995. https://doi.org/10.1073/pnas.1707517114.

5. He, M., Huang, T.-S., Li, S., Hong, H.-C., Chen, Z., Martin, M., Zhou, X., Huang, H.-Y., Su, S.-H., Zhang, J., et al. (2019). Atheroprotective Flow Upregulates ITPR3 (Inositol 1,4,5-Trisphosphate Receptor 3) in Vascular Endothelium via KLF4 (Krüppel-Like Factor 4)-Mediated Histone Modifications. Arteriosclerosis, Thrombosis, and Vascular Biology *39*, 902–914. https://doi.org/10.1161/ATVBAHA.118.312301.

6. Mendez, P.L., Obendorf, L., Jatzlau, J., Burdzinski, W., Reichenbach, M., Nageswaran, V., Haghikia, A., Stangl, V., Hiepen, C., and Knaus, P. (2022). Atheroprone fluid shear stress-regulated ALK1-Endoglin-SMAD signaling originates from early endosomes. BMC Biol. *20*, 210. https://doi.org/10.1186/s12915-022-01396-y.

7. Hiepen, C., Mendez, P.L., and Knaus, P. (2020). It Takes Two to Tango: Endothelial TGFbeta/BMP Signaling Crosstalk with Mechanobiology. Cells *9*. https://doi.org/10.3390/cells9091965.

8. Walshe, T.E., dela Paz, N.G., and D'Amore, P.A. (2013). The role of shear-induced transforming growth factor-β signaling in the endothelium. Arterioscler. Thromb. Vasc. Biol. *33*, 2608–2617. https://doi.org/10.1161/atvbaha.113.302161.

9. Baeyens, N., Larrivée, B., Ola, R., Hayward-Piatkowskyi, B., Dubrac, A., Huang, B., Ross, T.D., Coon, B.G., Min, E., Tsarfati, M., et al. (2016). Defective fluid shear stress mechanotransduction mediates hereditary hemorrhagic telangiectasia. J. Cell Biol. *214*, 807–816. https://doi.org/10.1083/jcb.201603106.

10. García de Vinuesa, A., Abdelilah-Seyfried, S., Knaus, P., Zwijsen, A., and Bailly, S. (2016). BMP signaling in vascular biology and dysfunction. Cytokine Growth Factor Rev. *27*, 65–79. https://doi.org/10.1016/j.cytogfr.2015.12.005.

11. Goumans, M.J., Zwijsen, A., Ten Dijke, P., and Bailly, S. (2018). Bone Morphogenetic Proteins in Vascular Homeostasis and Disease. Cold Spring Harb. Perspect. Biol. *10*, a031989. https://doi.org/10.1101/cshperspect.a031989.

12. Zhang, M., Sara, J.D., Wang, F.L., Liu, L.P., Su, L.X., Zhe, J., Wu, X., and Liu, J.H. (2015). Increased plasma BMP-2 levels are associated with atherosclerosis burden and coronary calcification in type 2 diabetic patients. Cardiovasc. Diabetol. *14*, 64. https://doi.org/10.1186/s12933-015-0214-3.

13. Tillet, E., Ouarné, M., Desroches-Castan, A., Mallet, C., Subileau, M., Didier, R., Lioutsko, A., Belthier, G., Feige, J.J., and Bailly, S. (2018). A heterodimer formed by bone morphogenetic protein 9 (BMP9) and BMP10 provides most BMP biological activity in plasma. J. Biol. Chem. *293*, 10963–10974. https://doi.org/10.1074/jbc.RA118.002968.

14. Gomez-Puerto, M.C., Iyengar, P.V., García de Vinuesa, A., Ten Dijke, P., and Sanchez-Duffhues, G. (2019). Bone morphogenetic protein receptor signal transduction in human disease. J. Pathol. *247*, 9–20. https://doi.org/10.1002/path.5170.

15. Benn, A., Hiepen, C., Osterland, M., Schütte, C., Zwijsen, A., and Knaus, P. (2017). Role of bone morphogenetic proteins in sprouting angiogenesis: differential BMP receptor-dependent signaling pathways balance stalk vs. tip cell competence. FASEB J *31*, 4720–4733. https://doi.org/10.1096/fj.201700193RR.

16. Morikawa, M., Koinuma, D., Tsutsumi, S., Vasilaki, E., Kanki, Y., Heldin, C.H., Aburatani, H., and Miyazono, K. (2011). ChIP-seq reveals cell type-specific binding patterns of BMP-specific Smads and a novel binding motif. Nucleic Acids Res. *39*, 8712–8727. https://doi.org/10.1093/nar/gkr572.

17. Larrivée, B., Prahst, C., Gordon, E., del Toro, R., Mathivet, T., Duarte, A., Simons, M., and Eichmann, A. (2012). ALK1 signaling inhibits angiogenesis by cooperating with the Notch pathway. Dev. Cell *22*, 489–500. https://doi.org/10.1016/j.devcel.2012.02.005.

18. Gkatzis, K., Thalgott, J., Dos-Santos-Luis, D., Martin, S., Lamandé, N., Carette, M.F., Disch, F., Snijder, R.J., Westermann, C.J., Mager, J.J., et al. (2016). Interaction Between ALK1 Signaling and Connexin40 in the Development of Arteriovenous Malformations. Arterioscl Throm Vas *36*, 707–717. https://doi.org/10.1161/Atvbaha.115.306719.

19. Akla, N., Viallard, C., Popovic, N., Lora Gil, C., Sapieha, P., and Larrivée, B. (2018). BMP9 (Bone Morphogenetic Protein-9)/Alk1 (Activin-Like Kinase Receptor Type I) Signaling Prevents Hyperglycemia-Induced Vascular Permeability. Arterioscl Throm Vas *38*, 1821–1836. https://doi.org/10.1161/Atvbaha.118.310733.

20. Rostama, B., Turner, J.E., Seavey, G.T., Norton, C.R., Gridley, T., Vary, C.P.H., and Liaw, L. (2015). DLL4/Notch1 and BMP9 Interdependent Signaling Induces Human Endothelial Cell Quiescence via P27KIP1 and Thrombospondin-1. Arterioscler. Thromb. Vasc. Biol. *35*, 2626–2637. https://doi.org/10.1161/ATVBAHA.115.306541.

21. David, L., Mallet, C., Keramidas, M., Lamandé, N., Gasc, J.M., Dupuis-Girod, S., Plauchu, H., Feige, J.J., and Bailly, S. (2008). Bone morphogenetic protein-9 is a circulating vascular quiescence factor. Circ. Res. *102*, 914–922. https://doi.org/10.1161/CIRCRESAHA.107.165530.

22. Martin-Malpartida, P., Batet, M., Kaczmarska, Z., Freier, R., Gomes, T., Aragón, E., Zou, Y., Wang, Q., Xi, Q., Ruiz, L.,

et al. (2017). Structural basis for genome wide recognition of 5-bp GC motifs by SMAD transcription factors. Nat. Commun. *8*, 2070. https://doi.org/10.1038/s41467-017-02054-6.

23. Shi, Y., Wang, Y.F., Jayaraman, L., Yang, H., Massagué, J., and Pavletich, N.P. (1998). Crystal structure of a Smad MH1 domain bound to DNA: insights on DNA binding in TGF-beta signaling. Cell *94*, 585–594.

24. Shi, Y., and Massagué, J. (2003). Mechanisms of TGF-beta signaling from cell membrane to the nucleus. Cell *113*, 685–700. https://doi.org/10.1016/s0092-8674(03)00432-x.

25. BabuRajendran, N., Palasingam, P., Narasimhan, K., Sun, W., Prabhakar, S., Jauch, R., and Kolatkar, P.R. (2010). Structure of Smad1 MH1/DNA complex reveals distinctive rearrangements of BMP and TGF-beta effectors. Nucleic Acids Res. *38*, 3477–3488. https://doi.org/10.1093/nar/gkq046.

26. Baburajendran, N., Jauch, R., Tan, C.Y.Z., Narasimhan, K., and Kolatkar, P.R. (2011). Structural basis for the cooperative DNA recognition by Smad4 MH1 dimers. Nucleic Acids Res. *39*, 8213–8222. https://doi.org/10.1093/nar/gkr500.

27. Macias, M.J., Martin-Malpartida, P., and Massagué, J. (2015). Structural determinants of Smad function in TGF-beta signaling. Trends Biochem. Sci. *40*, 296–308. https://doi.org/10.1016/j.tibs.2015.03.012.

28. Ruiz, L., Kaczmarska, Z., Gomes, T., Aragon, E., Torner, C., Freier, R., Baginski, B., Martin-Malpartida, P., de Martin Garrido, N., Marquez, J.A., et al. (2021). Unveiling the dimer/monomer propensities of Smad MH1-DNA complexes. Comput. Struct. Biotechnol. J. *19*, 632–646. https://doi.org/10.1016/j.csbj.2020.12.044.

29. Zaret, K.S., and Carroll, J.S. (2011). Pioneer transcription factors: establishing competence for gene expression. Genes Dev. *25*, 2227–2241. https://doi.org/10.1101/gad.176826.111.

30. Stevanovic, M., Drakulic, D., Lazic, A., Ninkovic, D.S., Schwirtlich, M., and Mojsin, M. (2021). SOX Transcription Factors as Important Regulators of Neuronal and Glial Differentiation During Nervous System Development and Adult Neurogenesis. Front. Mol. Neurosci. *14*, 654031. https://doi.org/10.3389/fnmol.2021.654031.

31. Demos, C., Johnson, J., Andueza, A., Park, C., Kim, Y., Villa-Roel, N., Kang, D.W., Kumar, S., and Jo, H. (2022). Sox13 is a novel flow-sensitive transcription factor that prevents inflammation by repressing chemokine expression in endothelial cells. Front. Cardiovasc. Med. *9*, 979745. https://doi.org/10.3389/fcvm.2022.979745.

32. Moonen, J.-R., Chappell, J., Shi, M., Shinohara, T., Li, D., Mumbach, M.R., Zhang, F., Nair, R.V., Nasser, J., Mai, D.H., et al. (2022). KLF4 recruits SWI/SNF to increase chromatin accessibility and reprogram the endothelial enhancer landscape under laminar shear stress. Nat. Commun. *13*, 4941. https://doi.org/10.1038/s41467-022-32566-9.

33. Thilo, F., Vorderwülbecke, B.J., Marki, A., Krueger, K., Liu, Y., Baumunk, D., Zakrzewicz, A., and Tepel, M. (2012). Pulsatile atheroprone shear stress affects the expression of transient receptor potential channels in human endothelial cells. Hypertension *59*, 1232–1240. https://doi.org/10.1161/HYPERTENSIONAHA.111.183608.

34. Hill, C.S. (2016). Transcriptional Control by the SMADs. Cold Spring Harb. Perspect. Biol. *8*, a022079. https://doi.org/10.1101/cshperspect.a022079.

35. Buenrostro, J.D., Giresi, P.G., Zaba, L.C., Chang, H.Y., and Greenleaf, W.J. (2013). Transposition of native chromatin for fast and sensitive epigenomic profiling of open chromatin, DNA-binding proteins and nucleosome position. Nat. Methods *10*, 1213–1218. https://doi.org/10.1038/nmeth.2688.

36. Scharpfenecker, M., van Dinther, M., Liu, Z., van Bezooijen, R.L., Zhao, Q., Pukac, L., Löwik, C.W.G.M., and ten Dijke, P. (2007). BMP-9 signals via ALK1 and inhibits bFGF-induced endothelial cell proliferation and VEGF-stimulated angiogenesis. J. Cell Sci. *120*, 964–972. https://doi.org/10.1242/jcs.002949.

37. Suzuki, Y., Ohga, N., Morishita, Y., Hida, K., Miyazono, K., and Watabe, T. (2010). BMP-9 induces proliferation of multiple types of endothelial cells in vitro and in vivo. J. Cell Sci. *123*, 1684–1692. https://doi.org/10.1242/jcs.061556.

38. Canali, S., Zumbrennen-Bullough, K.B., Core, A.B., Wang, C.Y., Nairz, M., Bouley, R., Swirski, F.K., and Babitt, J.L. (2017). Endothelial cells produce bone morphogenetic protein 6 required for iron homeostasis in mice. Blood *129*, 405–414. https://doi.org/10.1182/blood-2016-06-721571.

39. David, L., Feige, J.J., and Bailly, S. (2009). Emerging role of bone morphogenetic proteins in angiogenesis. Cytokine Growth F R *20*, 203–212. https://doi.org/10.1016/j.cytogfr.2009.05.001.

40. David, L., Mallet, C., Mazerbourg, S., Feige, J.J., and Bailly, S. (2007). Identification of BMP9 and BMP10 as functional activators of the orphan activin receptor-like kinase 1 (ALK1) in endothelial cells. Blood *109*, 1953–1961. https://doi.org/10.1182/blood-2006-07-034124.

41. Salmon, R.M., Guo, J., Wood, J.H., Tong, Z., Beech, J.S., Lawera, A., Yu, M., Grainger, D.J., Reckless, J., Morrell, N.W., and Li, W. (2020). Molecular basis of ALK1-mediated signalling by BMP9/BMP10 and their prodomain-bound forms. Nat. Commun. *11*, 1621. https://doi.org/10.1038/s41467-020-15425-3.

42. Jatzlau, J., Burdzinski, W., Trumpp, M., Obendorf, L., Roßmann, K., Ravn, K., Hyvönen, M., Bottanelli, F., Broichhagen, J., and Knaus, P. (2023). A versatile Halo- and SNAP-tagged BMP/TGFbeta receptor library for quantification of cell surface ligand binding. Commun. Biol. *6*, 34. https://doi.org/10.1038/s42003-022-04388-4.

43. Richter, A., Alexdottir, M.S., Magnus, S.H., Richter, T.R., Morikawa, M., Zwijsen, A., and Valdimarsdottir, G. (2019). EGFL7 Mediates BMP9-Induced Sprouting Angiogenesis of Endothelial Cells Derived from Human Embryonic Stem Cells. Stem Cell Rep. *12*, 1250–1259. https://doi.org/10.1016/j.stemcr.2019.04.022.

44. Morikawa, M., Mitani, Y., Holmborn, K., Kato, T., Koinuma, D., Maruyama, J., Vasilaki, E., Sawada, H., Kobayashi, M., Ozawa, T., et al. (2019). The ALK-1/SMAD/ATOH8 axis attenuates hypoxic responses and protects against the development of pulmonary arterial hypertension. Sci. Signal. *12*, eaay4430. https://doi.org/10.1126/scisignal.aay4430.

45. McLean, C.Y., Bristor, D., Hiller, M., Clarke, S.L., Schaar, B.T., Lowe, C.B., Wenger, A.M., and Bejerano, G. (2010). GREAT improves functional interpretation of cis-regulatory regions. Nat. Biotechnol. *28*, 495–501. https://doi.org/10.1038/nbt.1630.

46. Heinz, S., Benner, C., Spann, N., Bertolino, E., Lin, Y.C., Laslo, P., Cheng, J.X., Murre, C., Singh, H., and Glass, C.K. (2010). Simple combinations of lineage-determining transcription factors prime cis-regulatory elements required for macrophage and B cell identities. Mol. Cell *38*, 576–589. https://doi.org/10.1016/j.molcel.2010.05.004.

47. Dennler, S., Itoh, S., Vivien, D., ten Dijke, P., Huet, S., and Gauthier, J.M. (1998). Direct binding of Smad3 and Smad4 to critical TGF beta-inducible elements in the promoter of human plasminogen activator inhibitor-type 1 gene. EMBO J. *17*, 3091–3100. https://doi.org/10.1093/emboj/17.11.3091.

48. Bentsen, M., Goymann, P., Schultheis, H., Klee, K., Petrova, A., Wiegandt, R., Fust, A., Preussner, J., Kuenne, C., Braun, T., et al. (2020). ATAC-seq footprinting unravels kinetics of transcription factor binding during zygotic genome activation. Nat. Commun. *11*, 4267. https://doi.org/10.1038/s41467-020-18035-1.

49. Peacock, H.M., Tabibian, A., Criem, N., Caolo, V., Hamard, L., Deryckere, A., Haefliger, J.A., Kwak, B.R., Zwijsen, A., and Jones, E.A.V. (2020). Impaired SMAD1/5 Mechanotransduction and Cx37 (Connexin37) Expression Enable Pathological Vessel Enlargement and Shunting. Arterioscler. Thromb. Vasc. Biol. *40*, e87–e104. https://doi.org/10.1161/ATVBAHA.119.313122.

50. Vion, A.C., Alt, S., Klaus-Bergmann, A., Szymborska, A., Zheng, T., Perovic, T., Hammoutene, A., Oliveira, M.B., Bartels-Klein, E., Hollfinger, I., et al. (2018). Primary cilia sensitize endothelial cells to BMP and prevent excessive vascular regression. J. Cell Biol. *217*, 1651–1665. https://doi.org/10.1083/jcb.201706151.

51. Dekker, R.J., van Soest, S., Fontijn, R.D., Salamanca, S., de Groot, P.G., VanBavel, E., Pannekoek, H., and Horrevoets, A.J.G. (2002). Prolonged fluid shear stress induces a distinct set of endothelial cell genes, most specifically lung Krüppel-like factor (KLF2). Blood *100*, 1689–1698. https://doi.org/10.1182/blood-2002-01-0046.

52. Miyazono, K., Kamiya, Y., and Morikawa, M. (2010). Bone morphogenetic protein receptors and signal transduction. J. Biochem. *147*, 35–51. https://doi.org/10.1093/jb/mvp148.

53. Horbelt, D., Denkis, A., and Knaus, P. (2012). A portrait of Transforming Growth Factor beta superfamily signalling: Background matters. Int. J. Biochem. Cell Biol. *44*, 469–474. https://doi.org/10.1016/j.biocel.2011.12.013.

54. Morikawa, M., Koinuma, D., Miyazono, K., and Heldin, C.H. (2013). Genome-wide mechanisms of Smad binding. Oncogene *32*, 1609–1615. https://doi.org/10.1038/onc.2012.191.

55. Aragón, E., Wang, Q., Zou, Y., Morgani, S.M., Ruiz, L., Kaczmarska, Z., Su, J., Torner, C., Tian, L., Hu, J., et al. (2019). Structural basis for distinct roles of SMAD2 and SMAD3 in FOXH1 pioneer-directed TGF-beta signaling. Genes Dev. *33*, 1506–1524. https://doi.org/10.1101/gad.330837.119.

56. Hahn, C., and Schwartz, M.A. (2009). Mechanotransduction in vascular physiology and atherogenesis. Nat. Rev. Mol. Cell Biol. *10*, 53–62. https://doi.org/10.1038/nrm2596.

57. da Silva Madaleno, C., Jatzlau, J., and Knaus, P. (2020). BMP signalling in a mechanical context - Implications for bone biology. Bone *137*, 115416. https://doi.org/10.1016/j.bone.2020.115416.

58. Kanki, Y., Nakaki, R., Shimamura, T., Matsunaga, T., Yamamizu, K., Katayama, S., Suehiro, J.I., Osawa, T., Aburatani, H., Kodama, T., et al. (2017). Dynamically and epigenetically coordinated GATA/ETS/SOX transcription factor expression is indispensable for endothelial cell differentiation. Nucleic Acids Res. *45*, 4344–4358. https://doi.org/10.1093/nar/gkx159.

59. De Val, S., and Black, B.L. (2009). Transcriptional Control of Endothelial Cell Development. Dev. Cell *16*, 180–195. https://doi.org/10.1016/j.devcel.2009.01.014.

60. Gross, C.M., Aggarwal, S., Kumar, S., Tian, J., Kasa, A., Bogatcheva, N., Datar, S.A., Verin, A.D., Fineman, J.R., and Black, S.M. (2014). Sox18 preserves the pulmonary endothelial barrier under conditions of increased shear stress. J. Cell. Physiol. *229*, 1802–1816. https://doi.org/10.1002/jcp.24633.

61. Park, C.S., Kim, S.H., Yang, H.Y., Kim, J.H., Schermuly, R.T., Cho, Y.S., Kang, H., Park, J.H., Lee, E., Park, H., et al. (2022). Sox17 Deficiency Promotes Pulmonary Arterial Hypertension via HGF/c-Met Signaling. Circ. Res. *131*, 792–806. https://doi.org/10.1161/CIRCRESAHA.122.320845.

62. Lin, K.C., Yeh, J.N., Shao, P.L., Chiang, J.Y., Sung, P.H., Huang, C.R., Chen, Y.L., Yip, H.K., and Guo, J. (2023). Jaggeds/Notches promote endothelial-mesenchymal transition-mediated pulmonary arterial hypertension via upregulation of the expression of GATAs. J. Cell Mol. Med. *27*, 1110–1130. https://doi.org/10.1111/jcmm.17723.

63. Linnemann, A.K., O'Geen, H., Keles, S., Farnham, P.J., and Bresnick, E.H. (2011). Genetic framework for GATA factor function in vascular biology. Proc. Natl. Acad. Sci. USA *108*, 13641–13646. https://doi.org/10.1073/pnas.1108440108.

64. Nordin, K., and LaBonne, C. (2014). Sox5 Is a DNA-Binding Cofactor for BMP R-Smads that Directs Target Specificity during Patterning of the Early Ectoderm. Dev. Cell *31*, 374–382. https://doi.org/10.1016/j.devcel.2014.10.003.

65. Blokzijl, A., ten Dijke, P., and Ibáñez, C.F. (2002). Physical and functional interaction between GATA-3 and Smad3 allows TGF-beta regulation of GATA target genes. Curr. Biol. *12*, 35–45. https://doi.org/10.1016/S0960-9822(01)00623-6.

66. Zhao, B., Ye, X., Yu, J., Li, L., Li, W., Li, S., Yu, J., Lin, J.D., Wang, C.Y., Chinnaiyan, A.M., et al. (2008). TEAD mediates YAP-dependent gene induction and growth control. Genes Dev. *22*, 1962–1971. https://doi.org/10.1101/gad.1664408.

67. Cai, X., Wang, K.-C., and Meng, Z. (2021). Mechanoregulation of YAP and TAZ in Cellular Homeostasis and Disease Progression. Front. Cell Dev. Biol. *9*, 673599. https://doi.org/10.3389/fcell.2021.673599.

68. Alarcón, C., Zaromytidou, A.I., Xi, Q., Gao, S., Yu, J., Fujisawa, S., Barlas, A., Miller, A.N., Manova-Todorova, K., Macias, M.J., et al. (2009). Nuclear CDKs drive Smad transcriptional activation and turnover in BMP and TGF-beta pathways. Cell *139*, 757–769. https://doi.org/10.1016/j.cell.2009.09.035.

69. Szeto, S.G., Narimatsu, M., Lu, M., He, X., Sidiqi, A.M., Tolosa, M.F., Chan, L., De Freitas, K., Bialik, J.F., Majumder, S., et al. (2016). YAP/TAZ Are Mechanoregulators of TGF-β-Smad Signaling and Renal Fibrogenesis. J. Am. Soc. Nephrol. *27*, 3117–3128. https://doi.org/10.1681/asn.2015050499.

70. Boopathy, G.T.K., and Hong, W. (2019). Role of Hippo Pathway-YAP/TAZ Signaling in Angiogenesis. Front. Cell Dev. Biol. *7*, 49. UNSP 49. https://doi.org/10.3389/fcell.2019.00049.

71. Chai, N., Li, W.X., Wang, J., Wang, Z.X., Yang, S.M., and Wu, J.W. (2017). Structural basis for the Smad5 MH1 domain to recognize different DNA sequences. Nucleic Acids Res. *45*, 6255–6257. https://doi.org/10.1093/nar/gkx226.

72. Frankish, A., Diekhans, M., Ferreira, A.M., Johnson, R., Jungreis, I., Loveland, J., Mudge, J.M., Sisu, C., Wright, J., Armstrong, J., et al. (2019). GENCODE reference annotation for the human and mouse genomes. Nucleic Acids Res. *47*, D766–D773. https://doi.org/10.1093/nar/gky955.

73. Buenrostro, J.D., Wu, B., Litzenburger, U.M., Ruff, D., Gonzales, M.L., Snyder, M.P., Chang, H.Y., and Greenleaf, W.J. (2015). Single-cell chromatin accessibility reveals principles of regulatory variation. Nature *523*, 486–490. https://doi.org/10.1038/nature14590.

74. Lee, J. (2016). kundajelab/atac_dnase_pipelines: ATAC-seq and DNase-seq processing pipeline. https://github.com/kundajelab/atac_dnase_pipelines.

75. Langmead, B., and Salzberg, S.L. (2012). Fast gapped-read alignment with Bowtie 2. Nat. Methods *9*, 357–359. https://doi.org/10.1038/nmeth.1923.

76. Zhang, Y., Liu, T., Meyer, C.A., Eeckhoute, J., Johnson, D.S., Bernstein, B.E., Nusbaum, C., Myers, R.M., Brown, M., Li, W., and Liu, X.S. (2008). Model-based analysis of ChIP-Seq (MACS). Genome Biol. *9*, R137. https://doi.org/10.1186/gb-2008-9-9-r137.

77. Ramírez, F., Ryan, D.P., Grüning, B., Bhardwaj, V., Kilpert, F., Richter, A.S., Heyne, S., Dündar, F., and Manke, T. (2016). deepTools2: a next generation web server for deep-sequencing data analysis. Nucleic Acids Res. *44*, W160–W165. https://doi.org/10.1093/nar/gkw257.

78. Ross-Innes, C.S., Stark, R., Teschendorff, A.E., Holmes, K.A., Ali, H.R., Dunning, M.J., Brown, G.D., Gojis, O., Ellis, I.O., Green, A.R., et al. (2012). Differential oestrogen receptor binding is associated with clinical outcome in breast cancer. Nature *481*, 389–393. https://doi.org/10.1038/nature10730.

79. Stark, R.B.G. (2011). DiffBind: Differential Binding Analysis of ChIP-Seq Peak Data. http://bioconductor.org/packages/release/bioc/vignettes/DiffBind/inst/doc/DiffBind.pdf.

80. Lawrence, M., Huber, W., Pagès, H., Aboyoun, P., Carlson, M., Gentleman, R., Morgan, M.T., and Carey, V.J. (2013). Software for computing and annotating genomic ranges. PLoS Comput. Biol. *9*, e1003118. https://doi.org/10.1371/journal.pcbi.1003118.

81. Tanigawa, Y., Dyer, E.S., and Bejerano, G. (2022). WhichTF is functionally important in your open chromatin data? PLoS Comput. Biol. *18*, e1010378. https://doi.org/10.1371/journal.pcbi.1010378.

82. Quinlan, A.R., and Hall, I.M. (2010). BEDTools: a flexible suite of utilities for comparing genomic features. Bioinformatics *26*, 841–842. https://doi.org/10.1093/bioinformatics/btq033.

83. Buenrostro, J.D., Wu, B., Chang, H.Y., and Greenleaf, W.J. (2015). ATAC-seq: A Method for Assaying Chromatin Accessibility Genome-Wide. Curr. Protoc. Mol. Biol. *109*. 21-29.21.29.29. https://doi.org/10.1002/0471142727.mb2129s109.

84. Corces, M.R., Trevino, A.E., Hamilton, E.G., Greenside, P.G., Sinnott-Armstrong, N.A.,

Vesuna, S., Satpathy, A.T., Rubin, A.J., Montine, K.S., Wu, B., et al. (2017). An improved ATAC-seq protocol reduces background and enables interrogation of frozen tissues. Nat. Methods *14*, 959–962. https://doi.org/10.1038/nmeth.4396.

85. ENCODE Project Consortium, Kundaje, A., Aldred, S.F., Collins, P.J., Davis, C.A., Doyle, F., Epstein, C.B., Frietze, S., Harrow, J., Kaul, R., et al. (2012). An integrated encyclopedia of DNA elements in the human genome. Nature *489*, 57–74. https://doi.org/10.1038/nature11247.

86. Ross-Innes, C.S., Stark, R., Teschendorff, A.E., Holmes, K.A., Ali, H.R., Dunning, M.J., Brown, G.D., Gojis, O., Ellis, I.O., Green, A.R., et al. (2012). Differential oestrogen receptor binding is associated with clinical outcome in breast cancer. Nature *481*, 389–393. https://doi.org/10.1038/nature10730.

87. Stark, R., and Brown, G. (2011). DiffBind: Differential Binding Analysis of ChIP-Seq Peak Data (Bioconductor)).

STAR★METHODS

KEY RESOURCES TABLE

REAGENT or RESOURCE	SOURCE	IDENTIFIER
Antibodies		
Rabbit monoclonal anti-SMAD1	Cell Signaling Technology	Cat#6944; (D59D7); RRID: AB_10858882
Rabbit monoclonal anti-pSMAD1/5 (Ser463/465)	Cell Signaling Technology	Cat#9516; (41D10); RRID: AB_491015
Rabbit monoclonal anti-UNC5B	Cell Signaling Technology	Cat#13851; (D9M7Z)
Rabbit monoclonal anti-GAPDH	Cell Signaling Technology	Cat#2118; (14C10); RRID: AB_561053
Rabbit polyclonal anti-ID1	Santa Cruz	Cat#sc-488; (C-20); RRID: AB_631701
Goat IgG anti-rabbit IgG (H + L)-HRPO	Dianova	Cat#111-035-144; RRID: AB_2307391
Goat IgG anti-mouse IgG + IgM (H + L)-HRPO	Dianova	Cat#115-035-068; RRID: AB_2338505
Bacterial and virus strains		
DH5α Chemically Competent E. coli	Our lab	N/A
Chemicals, peptides, and recombinant proteins		
AMPure XP Beads	Beckmann Coulter	Cat#A63881
Lipofectamine2000	ThermoFisher Scientific	Cat#11668019
NEBNext®High-Fidelity 2X PCR Master Mix	New England BioLabs	Cat#M0541L
SYBR Green I	ThermoFisher Scientific	Cat#7563
Luna® Universal qPCR Master Mix	New England BioLabs	Cat#M3003L
M-MuLV reverse transcriptase enzyme	New England BioLabs	Cat#M0253S
rhBMP6	S. Vukicevic, Univ. of Zagreb, Croatia	N/A
rhBMP9/GDF2	PeproTech	Cat#120-07
Critical commercial assays		
QuickExtract™ DNA Extraction Solution	Lucigen	Cat#QE09050
WesternBright Quantum kit	Advansta	Cat#K-12042-D10
NucleoSpin RNA XS isolation kit	Macherey-Nagel	Cat#740902.50
MinElute Reaction Cleanup Kit	Qiagen	Cat#28206
Tagment DNA Enzyme and Buffer Large Kit	Illumina	Cat#20034198
Deposited data		
Human Genome Annotation GENCODE (v29 GRCh38.p12)	Frankish et al.[72]	https://www.gencodegenes.org/human/release_29.html
ATAC-seq data of BMP9, FSS and BMP9/FSS stimulated human Umbilical Artery Endothelial Cells (HUAECs)	This paper	https://www.ncbi.nlm.nih.gov/geo/query/acc.cgi?acc=GSE227588
SMAD1/5 ChIP-seq in BMP-9 treated HUVECs	Morikawa et al.[16]	https://www.ncbi.nlm.nih.gov/geo/query/acc.cgi?acc=GSE27661
SMAD1/5 ChIP-seq in BMP-9 treated HPAEC	Morikawa et al.[44]	https://www.ncbi.nlm.nih.gov/geo/query/acc.cgi?acc=GSE104682
Experimental models: Cell lines		
HEK293T cells	German Collection of Microorganisms and Cell Cultures (DSMZ)	Cat#ACC 635
Human Umbilical Artery Endothelial Cells (HUAECs), single donor, female	PromoCell	Cat#C-12200

(*Continued on next page*)

Continued

REAGENT or RESOURCE	SOURCE	IDENTIFIER
Oligonucleotides		
Accell human SMAD1 SMARTpool siRNA; Table S1	Dharmacon	Cat#E−012723-00-0005
Accell human SMAD5 SMARTpool siRNA; Table S1	Dharmacon	Cat#E−015791-00-0005
Accell Non-targeting Control siRNA #1; Table S1	Dharmacon	Cat#D-001910-01-05
ATAC-seq barcode adapters, Table S2	Buenrostro et al.[73] ordered at idtdna.com	N/A
Primers for cloning & Real-time PCR, Table S3	This paper, ordered at Thermo Fisher Scientific	N/A
Recombinant DNA		
pGL4.17[luc2/*Neo*]	Promega	Cat#E6721, DQ188837
pGL4.74[hRluc/TK]	Promega	Cat#E6921, AY738230
pGL4.17[luc2/*Neo*] containing SMAD1-bound regulatory regions 17,22,32 or 60k of human UNC5B	This paper	N/A
Software and algorithms		
Prism (v9.3)	GraphPad Software	https://www.graphpad.com/scientific-software/prism/
ENCODE ATAC-seq pipeline (v1.10.0)	Lee et al.[74]	https://github.com/ENCODE-DCC/atac-seq-pipeline#encode-atac-seq-pipeline
Bowtie2 (v2.3.4.3)	Langmead et al.[75]	https://bowtie-bio.sourceforge.net/bowtie2/index.shtml
MACS2 (v2.2.4)	Zhang et al.[76]	https://github.com/macs3-project/MACS/releases/tag/v2.2.4
deepTools (v3.5.1)	Ramírez et al.[77]	https://deeptools.readthedocs.io/en/develop/index.html
R (v4.0.5)	R Core Team	https://www.r-project.org/
R package DiffBind (v3.0)	Ross-Innes et al., Stark[78,79]	https://bioconductor.org/packages/release/bioc/html/DiffBind.html
R package GenomicRanges (v1.48.0)	Lawrence et al.[80]	https://bioconductor.org/packages/release/bioc/html/GenomicRanges.html
GREAT (v4.0.4)	McLean et al., Tanigawa[45,81]	http://great.stanford.edu/public/html/
HOMER (v4.11.1)	Heinz et al.[46]	http://homer.ucsd.edu/homer/
Bedtools (v2.29.2)	Quinlan and Hall[82]	https://bedtools.readthedocs.io/en/latest/
TOBIAS (v0.12.11)	Bentsen et al.[48]	https://github.com/loosolab/TOBIAS
Other		
µ-Slide I Luer 0.4 mm	ibidi	Cat#80176
ibidi Pump System	Ibidi	Cat#10902
HS DNA Bioanalyzer chip	Agilent	Cat#5067-4626
Perfusion Set YELLOW and GREEN	ibidi	10964
Gelatin from porcine skin, Type A	Sigma Aldrich	G2500

RESOURCE AVAILABILITY

Lead contact

Further information and requests for resources and reagents should be directed to and will be fulfilled by the lead contact, Petra Knaus (petra.knaus@fu-berlin.de).

Materials availability

Luciferase-Reporter constructs are available upon reasonable request.

Data and code availability

- ATAC-seq data have been deposited at GEO and are publicly available. This paper also analyzes existing, publicly available data. All accession numbers are listed in the key resources table.
- Original codes and scripts used for the analyses are publicly available as of the date of publication at GitHub: https://github.com/aybugealtay/BMP9_FSS_ATAC_analysis
- Any additional information required to reanalyze the data reported in this paper is available from the lead contact upon request.

EXPERIMENTAL MODEL AND SUBJECT DETAILS

Cell culture

For expansion female Human Umbilical Artery Endothelial Cells (HUAECs; PromoCell GmbH, Germany) were cultured in Endothelial Cell Growth Medium 2 (EGM2, C-22111, PromoCell GmbH, Germany) supplemented with 10% FCS, and penicillin (100 units/mL)/streptomycin (100 μg/mL) and analyzed between passages three and five. HEK293T cells were obtained from the German Collection of Microorganisms and Cell Cultures (DSMZ) and cultured in Dulbecco's Modified Eagle's Medium (DMEM) supplemented with 10% FCS, 2 mM L-glutamine and penicillin (100 units/mL)/streptomycin (100 μg/mL) (DMEM full medium) in a humidified atmosphere at 37°C and 5% CO_2 (v/v).

METHOD DETAILS

Transient transfection with expression plasmids and siRNA

All siRNAs were purchased from Dharmacon. For knockdown HUAECs were transfected with 40 nM Accell human SMAD1 SMARTpool, Accell human SMAD5 SMARTpool, or scrambled (Acell Non-targeting #1) siRNA with Lipofectamine2000 (ThermoFisher Scientific) according to manufacturer's instructions. In brief, 300.000 cells/6-well were seeded in 1 mL EGM2 full medium. On the following day, siRNA - Lipofactamine2000 mix was prepared in Opti-MEM - Reduced Serum Medium (ThermoFisher Scientific) and incubated for 20 min. Cells were washed with PBS once and 1 mL Opti-MEM was added. Next transfection mix was added to the cells. Subsequently, after 4 h 1 mL EGM2 medium was added, and 24 h later the medium replaced with fresh EGM2. All experiments were performed 48 h after siRNA transfection. For luciferase assays 50.000 HEK293T cells were seeded per 96-well and transfected with 50 ng firefly luciferase reporter construct and 30 ng RL-TK (Promega) using 0.8 μL Polyethylenimine (PEI, 2 μg/μL).

Cell stimulation with growth factors and SMI treatment

rhBMP6 (gift from S. Vukicevic, Univ. of Zagreb, Croatia) was reconstituted in MilliQ-H_20 and rhBMP9/GDF2 (PeproTech) was reconstituted in MilliQ-H_20 0.1% BSA. Both were stored at −80°C and added to the cells with the indicated concentrations in PBS after 3 h of starvation for cell stimulation, if not indicated otherwise.

SDS-PAGE & Western-blotting

For sodium dodecyl sulfate polyacrylamide gel-electrophoresis (SDS-PAGE), treated cells were lysed in 150 μL Laemmli buffer and frozen at −20°C. The lysate was pulled through an 18-gauge syringe and boiled for 10 min at 95°C. 10% polyacrylamide gels were cast in advance and stored at 4°C until usage. Separated by their molecular weight, proteins were transferred onto methanol-activated PVDF membranes by Western-blot. Membranes were blocked for 1 h in 0.1% TBS-T containing 3% w/v BSA, washed three times in 0.1% TBS-T and incubated with indicated primary antibodies overnight at 4°C. Primary antibodies were applied at a 1:1000 dilution in 3% w/v bovine serum albumin (BSA)/fraction V in TBST. For HRP-based detection, goat-α-mouse or goat-α-rabbit IgG HRP conjugates (±0.8 mg/mL, Dianova) were used at a dilution of 1:10,000. Chemiluminescent reactions were processed using WesternBright Quantum HRP substrate (advansta) and documented on a FUSION FX7 digital imaging system.

Quantitative real-time PCR

Cellular RNA was isolated using the NucleoSpin RNA XS isolation kit (Macherey-Nagel) according to the manufacturer's instructions. 0.5 to 1 μg total RNA was reversely transcribed by incubating it with random primers (100 pmol μL^{-1}, Invitrogen) and M-MuLV reverse transcriptase enzyme (200,000 U mL^{-1}, New England Biolabs) was added per sample. RT-PCR was performed using a StepOnePlus Real-Time PCR System (Thermo Fisher Scientific) with specific primers for the genes listed in Table S3. Reactions were performed in triplicates in MicroAmp Optical 96-well reaction plates (Thermo Fisher Scientific) using Luna PCR Master Mix (New England Biolabs). Fold induction was calculated by comparing relative gene expression to the housekeeping gene RSP9 using the ΔΔCT method.

Cloning of luciferase reporter constructs

To generate Firefly Luciferase reporter constructs carrying SMAD1-bound regulatory regions, human gDNA of HUAECs was isolated using QuickExtract DNA Extraction Solution (Lucigen) and the intronic regulatory regions (17, 22, 32 and 60) of *UNC5B* were PCR amplified using Phusion High-Fidelity DNA Polymerase (New England Biolabs) and subsequently purified, restriction digested and cloned into pGL4.17[luc2/*Neo*] (Promega).

Dual luciferase Reportergene assay

HEK293T cells were transfected with a luciferase reporter construct pGL4.17[luc2/*Neo*] (Promega, Germany) containing SMAD1-bound regulatory regions 17,22,32 or 60k of human UNC5B or BRE_2-luc. A constitutively expressing construct encoding renilla luciferase (RL-TK; Promega) was co-transfected as internal control. The next day, cells were starved in serum-free medium for 3 h and stimulated with 5 nM BMP6 overnight. Cell lysis was performed using passive lysis buffer (Promega) and measurement of luciferase activity was carried out according to manufacturer's instructions using a using a TECAN initiate f200 Luminometer (TECAN).

Application of fluid shear stress

$3*10^5$ cells were seeded in EBM-2 full medium (Basal Medium 2 and Supplement Pack (PromoCell, no. C-22111) supplemented with 1% P/S) to ibidi μ-Slide I Luer 0.4 mm (ibidi, no. 80176) pre-coated with 0.1% pork skin gelatin (Sigma-Aldrich). For static conditions, cells were seeded to an equal area in a 10 cm dish, restricted by a silicone barrier during gelatin coating and cell seeding. Cells were kept under culture conditions (37°C, 5% CO_2, 95% RH) for 48 h with daily medium exchanges. On the day of stimulation, medium was exchanged by pre-warmed EBM-2 starvation medium (Basal Medium 2 and Supplement Pack (PromoCell, no. C-22211) supplemented with 1% P/S and 2% FCS) and unidirectional laminar flow of 30 dyn/cm^2 was applied for 2 h or 6 h (subsequent to a 5 h ramp phase to allow call adaption to increasing shear stress). Shear stress was applied using the ibidi pump system (ibidi GmbH) with the associated software (v 1.4.2).

For co-stimulation experiments, BMP9 in PBS was added to pump reservoirs and static controls dishes at a final concentration of 0.3 nM. Cells were then harvested for RNA and ATAC-seq (2 h) or protein analysis (6 h).

ATAC-seq

For ATAC-seq, cells were cultured and exposed to stimulation conditions as described above. For maximum cell yield ibidi μ-slides channels were cut open with a scalpel. The resulting cut-out with the cells attached was transferred to a 10 cm culture dish. 200 μL pre-warmed trypsin was added and cells were incubated at 37°C. Cleavage reaction was stopped after 5 min with 800 μL of 10% FCS in PBS (4°C) and cell solution was collected.

For each sample 50.000 cells were transferred to a reaction tube and spun down *(500×g, 4°C, 5 min)*. Samples were kept on ice from now on. ATAC-seq[35,83] was performed as described in the section *transposition reaction* and buffers from Omni ATAC protocol[84] (see table. In brief, isolated cells were lysed in 50 μL lysis buffer for 3 min, 50 μL wash buffer added, spun down *(500×g, 4°C, 5 min)*, resuspended in 50 μL tagmentation buffer and incubated *(37°C, shaking @ 800 rpm, 30 min)*. This was followed by DNA purification with the MinElute Reaction Cleanup Kit (Qiagen, no. 28206). For clean-up, the manufacturers protocol was followed with two exceptions: Elution was done in 11 μL to get full 10 μL residual volume. Also, longer elution

time (3–5 min) was used for higher yield of DNA fragments. DNA concentration was measured with a Qubit fluorometer. DNA fragments were stored at −20°C until further processing.

ATAC-seq library preparation

Library generation, amplification and purification was conducted as in Buenrostro 2015,[78,79] including the qPCR step to estimate the appropriate number of additional PCR cycles. In brief, indexing primers v2_Ad1.2/3 and v2_Ad2.3/4/5/6 (2.5 μL each) from Buenrostro 2015a[73] were ligated to the DNA fragments (10μL + 10 μL H2O) using PCR Master Mix (NEB, M0541L) (25 μL) in a thermocycler (72°C, 5min; 98°C, 30 s; 5x (98°C, 10s; 63°C, 30 s; 72°C 1 min)). qPCR was conducted to determine final no. of PCR cycles with 5 μL Library, 2.5 μL H_2O, 0.5 μL Ad1.x, 0.5 μL Ad2.x, 1.5 μL 10x SYBR Green I (ThermoFisher Scientific, S7563), 5 μL PCR Master Mix with above settings for 20 cycles, skipping the initial 72°C, 5 min. The partially amplified libraries were then further cycled with above settings, according to the CT values from the qPCR. After that, two-sided size selection with magnetic AMPure XP Beads (Beckmann Coulter, no. A63881; 0.55× and 0.9× sample volume of bead solution added) was used to remove primer-dimers and large DNA fragments > 1kb. Library quality was assessed with an HS DNA Bioanalyzer chip (Agilent, no. 5067-4626) before 2 × 100 paired end Illumina high output sequencing (Max Planck Sequencing Core Facility at MPIMG).

ATAC-seq data preprocessing

ATAC-seq data were processedvia the standard ENCODE[85] ATAC-seq pipeline, using Caper with Conda (v1.10.0, https://github.com/ENCODE-DCC/atac-seq-pipeline/releases/tag/v1.10.0). Briefly, reads were aligned with Bowtie2 (v2.3.4.3)[75] to hg38 reference genome and filtered for unmapped, duplicates and mitochondrial reads. Peaks calling was performed using MACS2 (v2.2.4)[76] for each individual replicate.

We generated bigWig files for visualization purposes using bamCoverage (v3.5.1) module from deepTools[77] with parameters –normalizeUsing RPGC –effectiveGenomeSize 2913022398. We further used deepTools *computeMatrix* (v3.5.1) module with parameters –referencePoint center -a 1500 -b 1500 and *plotHeatmap* (v3.5.1) module with default parameters to generate heatmaps.

Differential accessibility analysis

We performed differential accessibility analysis for each condition using DiffBind R package (v3.0)[86,87] after sequencing depth normalization and by using DESeq2 as the underlying method. We identified significantly differential accessible regions by filtering for FDR $\leq$ 0.05 and fold change >1.5. Gene Ontology analysis of differentially accessible regions was performed with GREAT tool (v4.0.4)[45,81] in basal plus extension mode with default settings.

Transcription factor motif analysis

Motif enrichment analysis was performed using HOMER (v4.11.1)[46] with GENCODE v29 (Release 29, GRCh38.p12) genome annotation.[72] We used *findMotifsGenome* module with the parameters -size 200 -len 8 both for motif enrichment analysis and *de novo* motif discovery.

In order to count motif occurrences and check whether they form clusters, we used *annotatePeaks* module from HOMER[46] and obtained peak regions enriched for motif of interests, specifically, BGCSAGAC and CTGGCGCC (the motif files are included in the supplement). We then extracted the exact sequences of these peaks using bedtools (v2.29.2)[82] *getfasta* module and counted the occurrences.

Transcription factor footprinting analysis

We employed TOBIAS (v0.12.11)[48] framework to conduct the transcription factor (TF) footprinting analysis. We used the same genome and the motif database (obtained from HOMER) as for the motif enrichment analysis. To perform TF footprinting, we first corrected the Tn5 bias and normalized ATAC-seq signals using the ATACorrect tool of TOBIAS. Next, we used ScoreBigwig to scan footprints within the selected/differential peak regions (with fold change >1.5) and obtained footprint scores. TOBIAS BINDetect matched these footprints to the motif database. BINDetect was then used to compare the identified footprints and capture the differential binding activities across experimental conditions such as BMP9-knockout and the control sample in our project. Lastly, among all the TOBIAS-predicted differential TFs, we selected the most significantly differentially-binding 50 TFs with p values <0.01.

Figures

Schemes were created with BioRender.com and figures were assembled using Adobe Photoshop 2020.

QUANTIFICATION AND STATISTICAL ANALYSIS

Statistical tests were performed using GraphPad Prism (v9.3) software. All statistical tests are listed in the figure legends. Normal distributions of datasets were tested with the Shapiro-Wilk normality test. In cases of failure to reject the null hypothesis, the ANOVA and Tukey's, Dunnett's or Šídák's post-hoc test were used to check for statistical significance under the normality assumption. For all experiments statistical significance was assigned, with an alpha-level of $p < 0.05$.